

1 **The formation and mitigation of nitrate pollution:**  
2 **Comparison between urban and suburban environments**

3 Suxia Yang<sup>1,2</sup>, Bin Yuan<sup>1,2\*</sup>, Yuwen Peng<sup>1,2</sup>, Shan Huang<sup>1,2</sup>, Wei Chen<sup>3</sup>, Weiwei Hu<sup>3</sup>,  
4 Chenglei Pei<sup>3,4,5,6</sup>, Jun Zhou<sup>1,2</sup>, David D. Parrish<sup>1</sup>, Wenjie Wang<sup>7</sup>, Xianjun He<sup>1,2</sup>,  
5 Chunlei Cheng<sup>2,8</sup>, Xiaobing Li<sup>1,2</sup>, Xiaoyun Yang<sup>1,2</sup>, Yu Song<sup>7</sup>, Haichao Wang<sup>9</sup>, Jipeng  
6 Qi<sup>1,2</sup>, Baolin Wang<sup>10</sup>, Chen Wang<sup>10</sup>, Chaomin Wang<sup>1,2</sup>, Zelong Wang<sup>1,2</sup>, Tiange Li<sup>1,2</sup>,  
7 E Zheng<sup>1,2</sup>, Sihang Wang<sup>1,2</sup>, Caihong Wu<sup>1,2</sup>, Mingfu Cai<sup>1,2</sup>, Chenshuo Ye<sup>7</sup>, Wei Song<sup>3</sup>,  
8 Peng Cheng<sup>8</sup>, Duohong Chen<sup>6</sup>, Xinming Wang<sup>3</sup>, Zhanyi Zhang<sup>1,2</sup>, Xuemei Wang<sup>1,2</sup>,  
9 Junyu Zheng<sup>1,2</sup>, Min Shao<sup>1,2\*</sup>

10 <sup>1</sup>Institute for Environmental and Climate Research, Jinan University, Guangzhou  
11 511443, China

12 <sup>2</sup>Guangdong-Hongkong-Macau Joint Laboratory of Collaborative Innovation for  
13 Environmental Quality, Jinan University, Guangzhou 511443, China

14 <sup>3</sup>State Key Laboratory of Organic Geochemistry and Guangdong Key Laboratory of  
15 Environmental Protection and Resources Utilization, Guangzhou Institute of  
16 Geochemistry, Chinese Academy of Sciences, Guangzhou 510640, China

17 <sup>4</sup>CAS Center for Excellence in Deep Earth Science, Guangzhou, 510640, China

18 <sup>5</sup>University of Chinese Academy of Sciences, Beijing 100049, China

19 <sup>6</sup>Guangzhou Ecological and Environmental Monitoring Center of Guangdong  
20 Province, Guangzhou 510060, China

21 <sup>7</sup>State Joint Key Laboratory of Environmental Simulation and Pollution Control,  
22 College of Environmental Sciences and Engineering, Peking University, Beijing  
23 100871, China

24 <sup>8</sup>Institute of Mass Spectrometry and Atmospheric Environment, Guangdong  
25 Provincial Engineering Research Center for on-line Source Apportionment System of  
26 Air Pollution, Jinan University, Guangzhou 510632, China

27 <sup>9</sup>School of Atmospheric Sciences, Sun Yat-Sen University, Guangzhou 510275, China

28 <sup>10</sup>School of Environmental Science and Engineering, Qilu University of Technology,  
29 Jinan 250353, China

30

31 *\*Correspondence to:* Bin Yuan (byuan@jnu.edu.cn) and Min Shao  
32 (mshao@pku.edu.cn)

33

34 **Abstract.** Ambient nitrate has been of increasing concern in PM<sub>2.5</sub>, while there are  
35 still large uncertainties in quantifying the formation of nitrate aerosol. The formation  
36 pathways of nitrate aerosol at an urban site and a suburban site in the Pearl River Delta  
37 (PRD) are investigated using an observation-constrained box model. Throughout the  
38 campaigns, aerosol pollution episodes were constantly accompanied with the increase  
39 of nitrate concentrations and fractions at both urban and suburban sites. The simulations  
40 demonstrate that chemical reactions in the daytime and at night both contributed  
41 significantly to formation of nitrate in the boundary layer at the two sites. However,  
42 nighttime reactions predominately occurred aloft in the residual layer at the urban site  
43 and downward transport from the residual layer in the morning is an important source  
44 (53%) for surface nitrate at the urban site, whereas similar amounts of nitrate were  
45 produced in the nocturnal boundary layer and residual layer at the suburban site, which  
46 results in little downward transport of nitrate from the residual layer to the ground at  
47 the suburban site. We show that nitrate formation was in the volatile organic  
48 compounds (VOCs)-limited regime at the urban site, and in the transition regime at the  
49 suburban site, identical to the response of ozone at both sites. The reduction of VOCs  
50 emissions can be an efficient approach to mitigate nitrate in both urban and suburban  
51 areas through influencing hydroxyl radical (OH) and N<sub>2</sub>O<sub>5</sub> production, which will also  
52 be beneficial for the synergistic control of regional ozone pollution. The results  
53 highlight that the relative importance of nitrate formation pathways and ozone can be  
54 site-specific, and the quantitative understanding of various pathways of nitrate  
55 formation will provide insights for developing nitrate and ozone mitigation strategies.

56

57 **Keywords:** nitrate, ozone, volatile organic compounds, N<sub>2</sub>O<sub>5</sub>, formation pathways,  
58 urban and suburban sites

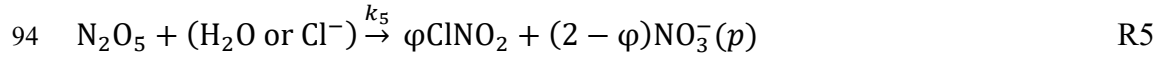
59

## 60 **1 Introduction**

61 Particulate nitrate is a substantial chemical component of fine particles, which  
62 plays a significant role in the acid deposition, visibility reduction, hygroscopic  
63 properties, and radiative forcing (Li et al., 1993; Watson, 2002; Pathak et al., 2009; Xu  
64 and Penner, 2012; Zhang et al., 2017; Liu et al., 2020). Due to the larger emission  
65 reduction of SO<sub>2</sub> than NO<sub>x</sub> and little change of NH<sub>3</sub> since the implementation of the  
66 clean air actions in China (Guo et al., 2018; Liu et al., 2019a; Zhai et al., 2021), a  
67 considerable increase in the nitrate fractions in aerosols has been observed in haze  
68 periods in the northern China Plain (Wen et al., 2018; Li et al., 2018; Lu et al., 2013; Fu  
69 et al., 2020), southern China (Pathak et al., 2009; Pathak et al., 2011) and eastern China  
70 (Griffith et al., 2015; Tao et al., 2018; Yun et al., 2018b; Li et al., 2018), which indicates  
71 the growing significance of nitrate in the formation of haze events. In addition, the  
72 photolysis of particulate nitrate can increase the production of sulfate and nitrous acid  
73 (HONO), implying the importance of nitrate in the synergetic enhancement of the  
74 atmospheric oxidizing capability in haze events (Gen et al., 2019; Zhang et al., 2020; Ye  
75 et al., 2016; Ye et al., 2017), although the photolysis of particulate nitrate to produce  
76 HONO still remains highly uncertain (Romer et al., 2018). Hence, identifying and  
77 understanding the driving factors of nitrate formation are essential to establishment of  
78 optimized mitigation policies for fine particles.

79 Particulate inorganic nitrate is primarily produced through two processes: the  
80 photochemical reaction of hydroxyl radical (OH) and NO<sub>2</sub> during daytime (R1) and  
81 the heterogeneous uptake of N<sub>2</sub>O<sub>5</sub> (R2–R5) during nighttime. The gaseous nitric acid  
82 (HNO<sub>3</sub>) is produced by the reaction of OH and NO<sub>2</sub>, and then reacts with ammonia  
83 (NH<sub>3</sub>) to form particulate nitrate (Stelson and Seinfeld, 1982). The partitioning process  
84 of HNO<sub>3</sub> between the gas and particle phase is regulated by ambient temperature (*T*),  
85 relative humidity (RH) (Mozurkewich, 1993), aerosol pH and the abundance of NH<sub>3</sub>  
86 (R7) (Xue et al., 2014a; Yun et al., 2018b; Franchin et al., 2018). The pH value within  
87 a certain range plays an important role in the gas-particle partitioning of nitrate, which  
88 significantly impacts the nitrate formation (Guo et al., 2018; Lawal et al., 2018; Nenes  
89 et al., 2020).

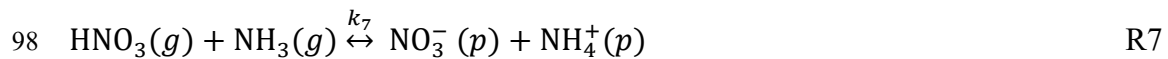




95  $k_5 = \frac{\omega l * \gamma * S_a}{4}$  (Eq.1)



97  $k_6 = J_{\text{ClNO}_2}$  (Eq.2)



99 The heterogeneous uptake reaction of  $\text{N}_2\text{O}_5$  can occur on the surface of water or  
 100 chlorine-containing particle (R5); and the reaction constant ( $k_5$ ) is described by Eq.1,  
 101 where  $\varphi$  is the production yield of  $\text{ClNO}_2$  in R5,  $\omega l$  is the average molecular speed of  
 102  $\text{N}_2\text{O}_5$  ( $\text{m s}^{-1}$ ),  $\gamma$  is the uptake coefficient of  $\text{N}_2\text{O}_5$  and  $S_a$  ( $\text{m}^2 \text{m}^{-3}$ ) is the aerosol surface  
 103 area concentration in Eq.1. The nitryl chloride ( $\text{ClNO}_2$ ) produced by the heterogeneous  
 104 uptake reaction of  $\text{N}_2\text{O}_5$  at night would photolysis in the next morning, which would  
 105 produce chlorine atom and  $\text{NO}_2$  (R6). Here the reaction rate  $k_6$  was denoted as the  
 106 photolysis rate of  $\text{ClNO}_2$  ( $J_{\text{ClNO}_2}$ ). The heterogeneous uptake reaction of  $\text{N}_2\text{O}_5$  is  
 107 affected by the uptake coefficient ( $\gamma$ ) and the production yield of  $\text{ClNO}_2$  ( $\varphi$ ), which  
 108 cannot be directly measured and are significantly impacted by the aerosol components  
 109 and ambient RH (Bertram and Thornton, 2009; Bian et al., 2017; McDuffie et al.,  
 110 2018a; McDuffie et al., 2018b). Thus, the nocturnal contribution to nitrate formation  
 111 still has great uncertainty.

112 With the radiative cooling in the afternoon, the mixed layer decoupled into a  
 113 steady, near surface nocturnal boundary layer (NBL) and a residual layer (RL), which  
 114 is a neutral layer and formed aloft during the turbulence attenuation process (Prabhakar  
 115 et al., 2017). The heterogeneous uptake of  $\text{N}_2\text{O}_5$  in the nocturnal boundary layer is  
 116 greatly disturbed in the presence of fresh  $\text{NO}$  emissions, which titrate the  $\text{NO}_3$  radical  
 117 within the stagnant boundary layer (Geyer and Stutz, 2004; Li et al., 2020; Chen et al.,  
 118 2020). However, aircraft observations in California and Utah in the US have revealed  
 119 that active uptake of  $\text{N}_2\text{O}_5$  in the residual layer contributed a major portion of the near-  
 120 surface nitrate accumulation during the morning transport from aloft (Brown et al.,  
 121 2006; Chow et al., 2006; Prabhakar et al., 2017; McDuffie et al., 2019; Womack et al.,

122 2019). Similarly, ground- and tower-based field observations also pointed out the  
123 important contribution of this pathway to the rapid increase of near-surface nitrate  
124 concentrations in Beijing, China (Wang et al., 2018a;Chen et al., 2020). However,  
125 under different atmospheric conditions, the relative importance of nitrate production  
126 varies significantly within the residual layer (McDuffie et al., 2019;Tang et al., 2021),  
127 giving widely varying relative contributions of the major chemical pathways to nitrate  
128 pollution among different sites (Wang et al., 2018a;Womack et al., 2019;Chen et al.,  
129 2020;Lin et al., 2020). A comprehensive understanding of the nitrate production in the  
130 residual layer is required to quantify the contributions of different formation pathways  
131 to nitrate pollution.

132 The nitrate production from the reaction of OH and NO<sub>2</sub> pathway during daytime  
133 is well-understood, and the control of NO<sub>x</sub> emission is commonly considered as an  
134 effective strategy to reduce ambient nitrate. However, several studies reported that the  
135 efficiency of NO<sub>x</sub> reduction in nitrate control is limited, and it may enhance nitrate  
136 production under some conditions (Womack et al., 2019;Dong et al., 2014;Hou et al.,  
137 2019). The study by Womack et al. (2019) showed that both nitrate and ozone were  
138 VOCs-limited in Salt Lake City, suggesting that VOCs control would effectively reduce  
139 nitrate. Similarly, modeling studies also found that the nitrate formation was more  
140 sensitive to the change in VOCs concentrations over the northern and eastern China  
141 (Dong et al., 2014;Lu et al., 2019;Fu et al., 2020). The sensitivity of nitrate production  
142 to both NO<sub>x</sub> and VOCs in different regions should be comparatively evaluated, which  
143 could provide helpful implications in formulating effective control strategies for the  
144 mitigation of aerosol pollution.

145 In recent years, the nitrate formation in haze episodes has been studied in northern  
146 China (Liu et al., 2015;Wang et al., 2017a;Wen et al., 2018;Fu et al., 2020;Chen et al.,  
147 2020), eastern China (Tao et al., 2016;Lin et al., 2020) and southern China (Qin et al.,  
148 2017;Tao et al., 2018;Yun et al., 2018b;Su et al., 2020), and the important contribution  
149 of the heterogeneous uptake of N<sub>2</sub>O<sub>5</sub> in the nighttime has been discussed (Wang et al.,  
150 2017b;Yun et al., 2018b;Yun et al., 2018a;Chen et al., 2020). However, these ground-  
151 based observations rarely considered the potential contributions of reactive uptake of  
152 N<sub>2</sub>O<sub>5</sub> aloft in the residual layer, which could be an important source of near-surface  
153 nitrate concentrations. In addition, few studies have comprehensively evaluated the  
154 relative influence of NO<sub>x</sub> and VOCs reductions on nitrate production in the urban and  
155 suburban areas (Hou et al., 2019).

156 In this study, we present the results from the ground- and tower-based  
157 measurements in both urban and suburban areas in southern China. An observation-  
158 constrained box model was used to simulate the production rates of nitrate from  
159 different formation pathways, and to compare the effects of reducing NO<sub>x</sub> and VOCs  
160 emissions in both urban and suburban areas. This work provides new insights into the  
161 synergetic mitigation of particle and ozone pollution, which can guide development of  
162 the most effective nitrate control strategies.

## 163 **2 Method and data**

### 164 **2.1 Field observation**

165 The ground-based field measurements were conducted at both an urban site in  
166 Guangzhou and a suburban site in Heshan. The tower-based measurements were  
167 conducted at an urban site in Guangzhou. The ground-based study in Guangzhou was  
168 carried out from late September to mid-November in 2018 at the Institute of  
169 Geochemistry (GIG), Chinese Academy of Sciences (23.1°N, 113.2°E), which is a  
170 typical urban site surrounded by a residential area and traffic avenues (Fig. 1). The  
171 instruments were deployed on the top of the 25-m building at GIG site. The ground-  
172 based measurement at the suburban site was performed from late September to mid-  
173 November in 2019 at the supersite of Heshan county (22.7°N, 112.9°E), which is  
174 approximately 50 km southwest to Foshan and 80 km southwest to Guangzhou, and is  
175 frequently influenced by anthropogenic emissions from upwind Guangzhou-Foshan  
176 mega-city areas. The tower-based measurements were conducted simultaneously at the  
177 ground and 448 m on the Canton Tower from late September to mid-November in 2018  
178 concurrent with the measurements at the GIG site, which are approximately 5.7 km  
179 apart each other (Fig. 1).

180 The chemical components of PM<sub>1</sub>, trace gases, and non-methane hydrocarbons  
181 (NMHC), and particle BC content and particle size distribution were both measured at  
182 the GIG and Heshan sites, whereas only trace gases (NO<sub>x</sub> and O<sub>3</sub>) and meteorological  
183 parameters were measured at the Canton Tower site. The non-refractory chemical  
184 compositions of PM<sub>1</sub> (NR-PM<sub>1</sub>), including organics (Org), sulfate (SO<sub>4</sub><sup>2-</sup>), nitrate  
185 (NO<sub>3</sub><sup>-</sup>), ammonium (NH<sub>4</sub><sup>+</sup>), and chloride (Cl<sup>-</sup>) were measured using a high-resolution  
186 time-of-flight aerosol mass spectrometer (HR-ToF-AMS, Aerodyne Research Inc., US)  
187 (Hu et al., 2016; Chen et al., 2021). Black carbon (BC) was measured using an

188 aethalometer (AE33, Magee Scientific Co., US). Particle number size distribution was  
189 measured using a scanning mobility particle sizer with an aerodynamic diameter  
190 ranging from 10 to 650 nm (SMPS, TSI, US) and aerosol particle sizer ranging from  
191 500 nm to 20  $\mu\text{m}$  (APS, TSI, US). Details on the limit of detection and accuracy of the  
192 instruments are presented in Table S1~ Table S3.

193  $\text{HNO}_3$ ,  $\text{N}_2\text{O}_5$ , and  $\text{ClNO}_2$  were measured using iodide-time-of-flight chemical  
194 ionization mass spectrometry (Iodide-TOF-CIMS, Aerodyne Research Inc., US) (Wang  
195 et al., 2020b; Ye et al., 2021). The non-methane hydrocarbons (NMHC) were measured  
196 using online GC-MS-FID (Wuhan Tianhong Co., Ltd, China) (Yuan et al., 2012) (Table  
197 S4). The concentrations of oxygenated VOCs (OVOCs), including formaldehyde  
198 (HCHO) and acetaldehyde ( $\text{CH}_3\text{CHO}$ ), the sum of methyl vinyl ketone (MVK) and  
199 methacrolein (MACR) were measured via a high-resolution proton transfer reaction  
200 time-of-flight mass spectrometry (PTR-ToF-MS, Ionicon Analytik, Austria) (Wang et  
201 al., 2020a; Wu et al., 2020). HONO was detected using a long path absorption  
202 photometer (LOPAP) at the GIG site (Yu et al., 2021), and was measured by the gas  
203 and aerosol collector (GAC) instrument at the Heshan site (Dong et al., 2012; Yang et  
204 al., 2014).  $\text{NH}_3$  was also measured by two sets of instruments: a cavity ring-down  
205 spectroscopy (CRDS, Picarro, US) was used at the GIG site and the GAC instrument  
206 was used at the Heshan site (von Bobruzki et al., 2010).

207 In addition, trace gases ( $\text{O}_3$  (49i),  $\text{NO}_x$  (42i), CO (48i) and  $\text{SO}_2$  (43i)) (Thermo  
208 Scientific, US) and meteorological parameters (i.e., wind speed (WS), wind direction  
209 (WD), temperature ( $T$ ), relative humidity (RH) and pressure ( $P$ )) (Vantage Pro 2, Davis  
210 Instruments Co., US) were simultaneously measured during these campaigns. The  
211 photolysis frequencies of  $\text{O}_3$ ,  $\text{NO}_2$ , HCHO, and HONO (PFS-100, Focused Photonics  
212 Inc., China) were also measured during the campaigns. Considering the integrity and  
213 temporal coverage of the measurements, we mainly focus on the investigated periods  
214 from October 7 to 29, 2018, at the GIG site and from October 16 to November 16, 2019,  
215 at the Heshan site.

## 216 **2.2 Box Model description**

217 A zero-dimensional observation-based box model (F0AM) (Wolfe et al., 2016)  
218 was used to simulate the production of nitrate in this study. The F0AM box model uses  
219 a subset of the Master Chemical Mechanism (MCM) v3.3.1 (Saunders et al.,

220 2003;Jenkin et al., 2003;Bloss et al., 2005), which explicitly describe chemical  
221 reactions of VOCs, RO<sub>x</sub> radicals (including OH, HO<sub>2</sub> and RO<sub>2</sub>), ozone and nitrate, and  
222 was widely used in laboratory and theoretical researches (Edwards et al.,  
223 2017;Anderson et al., 2017;D'Ambro et al., 2017;Womack et al., 2019).

224 In this study, the box model was constrained by observations of NMHCs, HCHO,  
225 CH<sub>3</sub>CHO, NO, CO, CH<sub>4</sub>, HONO, and meteorological parameters (i.e., photolysis rates,  
226 RH, *T* and *P*) measured at the GIG and Heshan sites. To investigate the convection of  
227 nitrate between the residual layer and the surface, the box model was split into two  
228 boxes at night (from 17:00 to 6:00 of the following morning) to separately represent the  
229 nocturnal boundary layer and the residual layer, respectively (Womack et al. (2019)  
230 (Fig. S1).

231 The simulation of the residual layer at the GIG site was constrained by the  
232 observation data from 488 m at the Canton Tower, while the simulation of the residual  
233 layer at the Heshan site was freely evolved from sunset time using the ground  
234 observation data of Heshan. The detailed model settings are described in Text S1, and  
235 the agreement between the observation data and simulations at the GIG and Canton  
236 Tower sites supports the use of similar simulation of the residual layer at the Heshan  
237 site. The model was operated in a time-dependent mode with a 5-min resolution. It was  
238 run for a 72-hour spin-up time to build steady-state concentrations for secondary  
239 pollutants that were not constrained during simulation. To prevent the build-up of long-  
240 lived species to unreasonable levels, an additional physical dilution process was applied  
241 in the model(Lu et al., 2017;Decker et al., 2019;Novak and Bertram, 2020;Liu et al.,  
242 2021;Yun et al., 2018b). To achieve agreement with the observation, a life time of 24  
243 h and 8 h were used at the GIG and Heshan site, respectively. The sensitivity tests with  
244 different dilution constant at the GIG and Heshan site were shown in Fig.S2 and Fig.S3,  
245 respectively. The background concentrations for ozone and CH<sub>4</sub> were set as 30 ppb and  
246 1.8 ppm, respectively (Wang et al., 2011).

247 The nocturnal production of nitrate from N<sub>2</sub>O<sub>5</sub> hydrolysis and the subsequent  
248 reactions (R5 and R6) are added to the box model.  $\gamma$  and  $\phi$  are calculated using the  
249 observation-based empirical parameterization method from Yu et al. (2020), where the  
250 impacts of nitrate, chloride, and aerosol liquid water content (ALWC) were evaluated  
251 to better represent the observed  $\gamma$ . The average values of  $\gamma$  were 0.018±0.01 and  
252 0.019±0.01 at the GIG and Heshan sites, respectively, which were comparable with the



253 observed mean data of  $\gamma$  ( $0.020\pm 0.019$ ) at the Heshan site in 2017. The  $\phi$  used in this  
 254 study were  $0.18\pm 0.15$  and  $0.20\pm 0.23$  at the GIG and Heshan sites, which were slightly  
 255 lower than the observed mean data of  $\phi$  at the Heshan site ( $0.31 \pm 0.27$ ) in 2017 (Yu et  
 256 al., 2020). The chemical compositions of fine particle were not measured at the Canton  
 257 Tower site, thus values of  $\gamma$  and  $\phi$  in the residual layer were assigned equal to those of  
 258 the nocturnal boundary layer. The  $\gamma$  and  $\phi$  exhibited complicated nonlinear dependence  
 259 on aerosol composition, aerosol liquid water and RH (Bertram and Thornton,  
 260 2009; McDuffie et al., 2019; Yu et al., 2020), such that  $\gamma$  and  $\phi$  has positive and negative  
 261 dependence with RH, respectively. There was higher RH, and lower chloride at the 488  
 262 m site, compared to the ground site of Canton Tower. The nitrate concentration was  
 263 comparable at the 488 m site to the ground site in the study of Zhou et al. (2020).  
 264 Combined with the higher RH and lower  $PM_{2.5}$  concentrations in the residual layer in  
 265 this study (as shown in Fig.S4), we inferred the negative deviations for  $\gamma$  and positive  
 266 deviations for  $\phi$  in the residual layer. The dry aerosol surface area concentration ( $S_a$ )  
 267 was calculated from the particle number size distribution and calibrated to the actual  
 268 atmospheric  $S_a$  using the RH-dependent hygroscopic growth factor ( $f(RH)$ ). The  $f(RH)$   
 269 was estimated from the aerosol composition measured by AMS and the aerosol liquid  
 270 water content, which included the inorganic-associated and organic-associated water.  
 271 The sum of inorganic-associated water estimated from ISORROPIA thermodynamic  
 272 model and organic-associated water estimated from the dry organic aerosol mass, was  
 273 used to calculate the growth of wet matter contributions, as described in the study of  
 274 McDuffie et al. (2018a).  $J_{ClNO_2}$  was scaled from measured  $NO_2$  photolysis frequencies  
 275 divided by a factor of 30 (Riedel et al., 2014).

276 The equilibrium coefficient between  $HNO_3$  and particulate nitrate is incorporated  
 277 into the box model as a pseudo-first-order reaction (Eq.3 and 4) through the equilibrium  
 278 absorption partitioning theory (Jacob, 2000; Yuan et al., 2016):



$$280 \quad k_{gf} = \left( \frac{R_a}{D_g} + \frac{4}{\omega * \alpha} \right)^{-1} * S_a \quad (Eq.3)$$

$$281 \quad k_{gb} = \left( \frac{R_a}{D_g} + \frac{4}{\omega * \alpha} \right)^{-1} \frac{S_a}{K_{eq}} \quad (Eq.4)$$

282 where  $R_a$  is the radius of nitrate particles (m),  $D_g$  is the gas-phase molecular diffusion  
 283 coefficient ( $m^2 s^{-1}$ ),  $\omega$  is the mean molecular speed of  $HNO_3$  ( $m s^{-1}$ ),  $\alpha$  is the mass

284 accommodation coefficient of  $\text{HNO}_3$ , and  $K_{eq}$  represents the equilibrium constant of  
285  $\text{HNO}_3$  and nitrate. These coefficients are the same as those in the chemical aqueous-  
286 phase radical mechanism (CAPRAM) (Ervens et al., 2003; Wen et al., 2015).

287 The empirical kinetic modeling approach (EKMA) is used here to identify the  
288 sensitivity of ozone and nitrate to the variations of  $\text{NO}_x$  and VOCs. The observed  
289 diurnal average conditions are used as the input for the base simulation. Sensitivity tests  
290 are conducted by increasing and decreasing initial anthropogenic VOCs (AVOCs) and  
291  $\text{NO}_x$  concentrations by a ratio ranging from 0.1 to 2.0 with 20 equal-distance steps  
292 without changing other parameters in the model (Tan et al., 2018; Lyu et al.,  
293 2019; Womack et al., 2019). The maximum concentration of ozone and nitrate in each  
294 scenario are plotted to generate the contour plots of the respective isopleths. Isoprene  
295 was included in the simulation as biogenic VOC (BVOC). Reducing BVOCs such as  
296 isoprene is impractical, so it is not scaled with AVOCs concentrations in the sensitivity  
297 simulations on control of precursors.

298 Since the  $\text{N}_2\text{O}_5$  is affected by the chemistry between ozone and VOCs,  
299 constraining  $\text{N}_2\text{O}_5$  concentrations with the change in  $\text{NO}_x$  ratio arbitrarily during the  
300 isopleth simulations is improper. Thus, we set the simulation of base case (S0) without  
301  $\text{N}_2\text{O}_5$  constrained. To evaluate the results of the base case, we design another simulation  
302 with  $\text{N}_2\text{O}_5$  constrained (S1) and compare the two simulated nitrate with the observation  
303 in Fig. S5. The model scenarios were described in Table S5 in detail. The base case  
304 simulation (S0) was comparable to the observation. The simulated nitrate with  $\text{N}_2\text{O}_5$   
305 constrained (S1) during October 9 to 10, 2018 was observed to be much higher  
306 compared to both the observations and base case simulation (S0) at the GIG site, which  
307 suggest that high concentrations of ambient  $\text{N}_2\text{O}_5$  measured during this short period  
308 may not contribute significantly to nitrate formation (Fig. S6). Overall, the simulated  
309 nitrate of base case without  $\text{N}_2\text{O}_5$  constrained agreed well with the observation  
310 suggesting the robustness of the model simulations.

311 Gaussian error propagation was used to evaluate the uncertainties about  
312 measurement parameters and reaction rates in the model, as described in Lu et al. (2012).  
313 The uncertainties of various measurement parameters (VOCs, trace gases,  
314 meteorological parameters, etc.) ranged from 0 to 20%, and uncertainties of reaction  
315 rates are in the order of ~20% (Lu et al., 2012).

## 316 **3 Results and discussion**

### 317 **3.1 Overview of nitrate concentrations during the campaign**

318 The temporal variations of mass concentrations of the major chemical components  
319 in PM<sub>1</sub> are shown in Fig. 2. The mean concentration of PM<sub>1</sub> was 41.7±23.1 μg m<sup>-3</sup> at  
320 the GIG site during the investigated period, which was comparable with that at the  
321 Heshan site (40.6 ±15.5 μg m<sup>-3</sup>). The aerosol composition differed between sites, with  
322 inorganic ions (sulfate, nitrate, and ammonia) higher and organic matter lower at the  
323 GIG site compared to the Heshan site.

324 Although the mass concentrations at the two sites were comparable, the mass  
325 fraction of nitrate in PM<sub>1</sub> at the GIG site increased from 10% to 33% as the mass  
326 concentration of PM<sub>1</sub> increased from 20 to 130 μg m<sup>-3</sup> (Fig. 3), while the fraction of  
327 nitrate increased from 10% to 20% at the Heshan site, suggesting that nitrate plays a  
328 more important role in the increase in PM<sub>1</sub> at the urban site than that at the suburban  
329 site. The significant increasing ratio of nitrate fraction from clean condition to polluted  
330 condition (~ 43%) was also revealed in the airborne observation in Utah Valley, US  
331 (Franchin et al., 2018). In addition, although the concentration of sulfate was higher  
332 than that of nitrate during most of the sampling periods, as PM<sub>1</sub> increased the mass  
333 concentration ratio of nitrate/sulfate increased from 0.5 to 2.0 at the GIG site and from  
334 0.5 to 1.5 at the Heshan site. The higher ratios of nitrate/sulfate during the polluted  
335 periods implies that reducing nitrate may be essential for reducing the occurrence of  
336 PM pollution in southern China. The increasing contributions of nitrate to PM<sub>1</sub> in this  
337 study were similar with those observed in northern China during haze pollution (Yang  
338 et al., 2017;Fu et al., 2020;Wen et al., 2015;Liu et al., 2015), suggesting the significance  
339 of nitrate mitigation to further reduce mass concentrations of fine particles in China.

340 The diurnal patterns of mean nitrate, NH<sub>3</sub>, NO<sub>2</sub> and HNO<sub>3</sub> concentrations observed  
341 at the GIG and Heshan sites are shown in Fig. 4. The highest nitrate concentration was  
342 observed in the morning at the GIG site and during nighttime at the Heshan site,  
343 suggesting differences in the processes that dominated the formation of nitrate at the  
344 two sites. At the GIG site, nitrate rapidly increased from 4:00 to 9:00, but the  
345 concentrations of NH<sub>3</sub> and HNO<sub>3</sub> increased slowly, which suggests the minor  
346 contribution of direct production of HNO<sub>3</sub> from the reaction of OH and NO<sub>2</sub>. The  
347 increase of nitrate during this period might be associated with the downward transport  
348 from the residual layer to the ground. The diurnal variations in O<sub>3</sub> and NO<sub>x</sub> measured

349 at the GIG and Canton Tower sites are shown in Fig. 5. The ground-based observations  
350 at the Canton Tower showed similar variation patterns of O<sub>3</sub> and NO<sub>x</sub> to the GIG site.  
351 However, the average concentration of O<sub>3</sub> at 488 m of Canton Tower site was 2.4 times  
352 higher than that at the GIG site during nighttime, and the lower nocturnal concentrations  
353 of NO (nearly zero) at the 488 m site would enhance the production of NO<sub>3</sub> and N<sub>2</sub>O<sub>5</sub>  
354 (Wang et al., 2018b; McDuffie et al., 2019). Therefore, heterogeneous uptake of N<sub>2</sub>O<sub>5</sub>  
355 during nighttime may be active at 488 m at urban site, which will be further investigated  
356 in Section 3.2. At the Heshan site, nitrate increased sharply in the early nighttime  
357 (before midnight), which may be attributable to the shallow nocturnal boundary layer  
358 or the enhanced nocturnal N<sub>2</sub>O<sub>5</sub> heterogeneous uptake reactions. Subsequently, there  
359 was a significant increase in nitrate from 7:00 to 9:00. The concentration of NH<sub>3</sub>  
360 showed variation pattern that was similar with that of nitrate and increased after 7:00,  
361 while the concentrations of HNO<sub>3</sub> and NO<sub>2</sub> showed a decreasing trend from 7:00 to  
362 9:00 at the Heshan site. The different growth characteristics of nitrate and the variation  
363 patterns of precursors at the two sites may be related to different formation processes,  
364 which will be discussed in detail later.

365 In this study, the wind speeds in the investigated periods at the GIG and Heshan  
366 sites were generally below 2 m s<sup>-1</sup> (Table S6), which suggests that regional transport  
367 may have limited contributions to the abundance of nitrate at the observation sites.  
368 Therefore, the discussion of the chemical formation process of nitrate in this study  
369 focuses on local production.

370 The molar ratios of [NH<sub>4</sub><sup>+</sup>] to the sum of 2×[SO<sub>4</sub><sup>2-</sup>]+[NO<sub>3</sub><sup>-</sup>] are calculated (Fig. S7)  
371 to determine whether there was enough NH<sub>4</sub><sup>+</sup> to neutralize nitrate. The molar ratios  
372 were approximately 1.0 at both GIG and Heshan sites, suggesting both NH<sub>3</sub> and HNO<sub>3</sub>  
373 were crucial precursors for nitrate formation. Based on these discussions, we will  
374 discuss the NH<sub>3</sub> effect on the nitrate partitioning firstly by thermodynamic  
375 ISORROPIA II model. The nitrate chemical formation pathways, which is mainly  
376 attributable to the production of HNO<sub>3</sub> and/or heterogeneous uptake of N<sub>2</sub>O<sub>5</sub> combining  
377 the box model, will be discussed in Sec. 3.2.

378 The ISORROPIA II model setting is described in Test S2 in detail. The  
379 ISORROPIA II modeled results of nitrate, ammonium, HNO<sub>3</sub>, and NH<sub>3</sub> at the GIG and  
380 Heshan site were displayed in Fig.S8 ~ Fig.S9. The particle-phase nitrate and  
381 ammonium at the GIG site showed a bit overestimation, while the gas-phase HNO<sub>3</sub>,  
382 and NH<sub>3</sub> showed overestimation at the Heshan site. Overall, the simulated components

383 showed good correlations with the observed concentrations at both sites. We use the  
384 ISORROPIA II model results to evaluate the particle fraction of nitrate in the sum of  
385  $\text{HNO}_3$ +nitrate ( $\epsilon(\text{NO}_3^-)$ ) against aerosol pH. Aerosol pH, which depends on the aerosol  
386 acidity and water content, is calculated by the following equation:

$$387 \text{ pH} = -\log_{10} \frac{1000 H_{air}^+}{\text{ALWC}} \quad (\text{Eq.5})$$

388 where  $H_{air}^+$  ( $\mu\text{g m}^{-3}$ ) is the hydronium concentration of the equilibrium particle and  
389 ALWC ( $\mu\text{g m}^{-3}$ ) is the aerosol water content from ISORROPIA II simulation.

390 The  $\epsilon(\text{NO}_3^-)$  against pH at the GIG and Heshan site are shown in Fig.6. The pH  
391 data are colored by relative humidity and fit to an “s-curve” as in Guo et al. (2018). The  
392 clustering of pH data mainly located between 1~3, and the  $\epsilon(\text{NO}_3^-)$  are sensitive to the  
393 change of pH. To further evaluate the sensitivity of  $\text{NH}_3$  and sulfate on this effect, the  
394 input of total ammonium ( $\text{NH}_x$ , ammonium +  $\text{NH}_3$ ) and sulfate were reduced from 10%  
395 to 90% relative to the ISORROPIA II base model, respectively, while keeping other  
396 parameters constant. The response of simulated nitrate concentration and aerosol pH to  
397 changes in  $\text{NH}_x$  and  $\text{SO}_4^{2-}$  are shown in Fig.7. The nitrate concentration decreased with  
398 the reduction of  $\text{NH}_x$ , and had little variation with the reduction of  $\text{SO}_4^{2-}$  (Fig.7 (a ~ b))  
399 at both sites. Along with the reduction of  $\text{NH}_x$ , the pH values decreased significantly  
400 (Fig.7 (c ~ d)), which caused the further decrease of  $\epsilon(\text{NO}_3^-)$ . The pH values showed a  
401 bit increase with the reduction of  $\text{SO}_4^{2-}$ , which may be caused by that there would be  
402 more available ammonium neutralized the hydronium. It is consistent with the study of  
403 Guo et al. (2018) and Nenes et al. (2020), suggesting the partitioning of nitrate was also  
404 affected by the  $\text{NH}_3$  in the pH values between 1~3. Thus, the control of  $\text{NH}_3$  is effective  
405 for the reduction of nitrate by affecting the partitioning process of nitrate at both GIG  
406 and Heshan site in this study. The partitioning of nitrate increased with the reduction of  
407 sulfate suggests the limited role of sulfate reduction on the mitigation of nitrate.

### 408 **3.2 Contributions of different pathways to nitrate formation**

409 To further investigate the chemical formation pathways of nitrate, which related  
410 to the photochemical and heterogeneous reactions, we adopt the box model results to  
411 simulate the contribution of different pathways to nitrate formation. The temporal  
412 variations in simulated and observed nitrate concentrations at the GIG and Heshan sites  
413 are presented in Fig. 8; simulated and observed nitrate showed similar concentrations  
414 and variation patterns. The diurnal variation of simulated nitrate is compared with the

415 observation in Fig.S10. The diurnal simulated nitrate was comparable with the  
416 observation at the GIG site, especially when considering the vertical transport from the  
417 residual layer in the morning. Unlike the GIG site, the diurnal simulated nitrate  
418 performed higher in the daytime, and little bit lower in the late nighttime, compared  
419 with the observation. It may be related to the lack of quantitative transport in the box  
420 model. The box model performance was evaluated using the mean bias (MB), index of  
421 agreement (IOA), and correlation coefficient ( $r$ ) (Table S7) (Liu et al., 2019b;Lyu et al.,  
422 2017;Wang et al., 2019;Curci et al., 2015). The IOA was larger than 0.7 and  $r$  was larger  
423 than 0.5 at both sites, indicating good agreements between simulated and observed  
424 nitrate concentrations. The temporal variations in simulated  $N_2O_5$  and  $ClNO_2$   
425 concentrations were higher than the observations at the Heshan site as shown in Fig. S6  
426 (c, d), the simulated results at the GIG site from October 9 to 10 were significantly  
427 lower than the observations (Fig.S6 (a, b)). The abnormally high observed  
428 concentrations of  $N_2O_5$  and  $ClNO_2$  that lasted for short periods (10-30 minutes) at the  
429 GIG site may be caused by transported air masses from upwind regions or vertical  
430 transport without well-mixed with fresh urban NO emissions. Simulation of these near-  
431 instantaneous processes transported to the site using a box model is difficult, as box  
432 model is more suitable to simulate the well-mixed air mass with little transport effects.  
433 However, the simulated nitrate concentrations without observed  $N_2O_5$  constrained was  
434 adequately comparable with the observations as shown in Fig. S5, implying the  
435 influence of the instantaneously high concentrations of  $N_2O_5$  on nitrate formation was  
436 negligible at the GIG site.

437       Based on these simulation results, we calculated the daily-averaged contributions  
438 of the two different reaction pathways to the nitrate concentration - the daytime  
439 production from  $OH + NO_2$  reaction and the nighttime production from  $N_2O_5$  uptake  
440 reaction in the nocturnal boundary layer and in the residual layer. The nitrate produced  
441 in the residual layer is only gradually mixed to the surface as the boundary layer  
442 develops during the following morning, while the nitrate contributed to the boundary  
443 layer column concentration always included the  $N_2O_5$  uptake in the residual layer during  
444 the whole nighttime (Wang et al., 2018a;Womack et al., 2019). The calculation methods  
445 to determine contribution to the boundary layer column concentrations and to ground-  
446 level nitrate concentrations should be distinguished.

447       To calculate the contribution to the boundary layer column concentration, the  
448 integral of the nitrate production rate from  $N_2O_5$  uptake from both the nocturnal surface

449 layer and the residual layer directly contribute to nitrate column concentrations layer  
450 during the whole nighttime, weighted as 0.4 and 0.6 based on their altitude fractions of  
451 the two layers, respectively. This calculation for the contributions to column  
452 concentration is the same as the methods presented by Wang et al. (2018a) and Womack  
453 et al. (2019). However, to quantify the contribution of nitrate produced from the  
454 residual layer to the ground nitrate concentration, one must account for the dynamic  
455 exchange between the residual layer and the surface-based boundary layer that develops  
456 during daytime. The integral time for this dynamic exchange was assumed from 6:00  
457 to 10:00 in the morning. Detailed descriptions of the calculations are provided in Text  
458 S3 in Supplementary Materials. The calculation about partitioning process from OH  
459 and NO<sub>2</sub> reaction in the daytime was the same in the two methods mentioned above,  
460 which was the partition part of the integral of the OH and NO<sub>2</sub> reaction during the  
461 daytime.

462 The contributions of nitrate to the boundary layer column concentration (i.e.  
463 average from ground to 1000 m) are shown in Fig. 9a. The contribution of nitrate  
464 production rate from N<sub>2</sub>O<sub>5</sub> uptake in the residual layer was 17.9 μg m<sup>-3</sup> day<sup>-1</sup> at the GIG  
465 site, which was much greater than the N<sub>2</sub>O<sub>5</sub> uptake in the nocturnal boundary layer (0.4  
466 μg m<sup>-3</sup> day<sup>-1</sup>). This may be caused by the fresh NO surface emissions, which titrate the  
467 NO<sub>3</sub> radical and ozone in the nocturnal boundary layer, as the mean NO concentration  
468 during the nighttime at the GIG site was 12.1 ppb. The contribution from nocturnal  
469 nitrate production in the boundary layer was comparable with the contribution from OH  
470 and NO<sub>2</sub> reaction (13.2 μg m<sup>-3</sup> day<sup>-1</sup>) during the daytime. In contrast to the GIG site,  
471 the contribution of nitrate production rate from N<sub>2</sub>O<sub>5</sub> uptake in the nocturnal boundary  
472 layer (6.2 μg m<sup>-3</sup> day<sup>-1</sup>) was comparable with that in the residual layer (4.4 μg m<sup>-3</sup> day<sup>-1</sup>)  
473 at the Heshan site. The similar nitrate concentration and production rate from N<sub>2</sub>O<sub>5</sub>  
474 uptake between the nocturnal boundary layer and residual layer in Fig.S12 (c, d) was  
475 due to smaller NO emissions at the Heshan site. The results demonstrate that nocturnal  
476 nitrate production plays an important role in nitrate production in the boundary layer,  
477 with nighttime contributions of 58% at the urban site and 35% at the suburban site.

478 The relative magnitudes of the contributions to the daily-averaged surface nitrate  
479 differ somewhat from the contributions to the entire boundary layer. The contributions  
480 from the three major pathways to surface nitrate concentrations at the two sites are  
481 compared in Fig. 9b. At the GIG site the nitrate production rate from the OH and NO<sub>2</sub>

482 reaction and downward transport from the residual layer were  $13.2 \mu\text{g m}^{-3} \text{ day}^{-1}$  and  
483  $16.6 \mu\text{g m}^{-3} \text{ day}^{-1}$ , contributing 43% and 53% of ground-level nitrate concentrations,  
484 with a minor contribution ( $1.1 \mu\text{g m}^{-3} \text{ day}^{-1}$ ) from the production of  $\text{N}_2\text{O}_5$  uptake in the  
485 nocturnal boundary layer. This is similar with the results in Fig.9a, implying a large  
486 nitrate contribution from  $\text{N}_2\text{O}_5$  uptake in the residual layer, but not in the nocturnal  
487 boundary layer at the urban site.

488 However, at the suburban Heshan site (Fig.9b), downward transport from the  
489 residual layer made no contribution to the surface nitrate concentration, which was  
490 smaller than the contribution of nitrate from the residual layer in Fig. 9a. This is due to  
491 the similar nitrate production rate from  $\text{N}_2\text{O}_5$  uptake between the nocturnal boundary  
492 layer and residual layer (see Fig. S12), inducing negligible convection between the two  
493 layers as the result of small concentration gradient (Brown et al., 2003; Baasandorj et  
494 al., 2017; Prabhakar et al., 2017). The nitrate production rate from OH and  $\text{NO}_2$  reaction  
495 ( $19.9 \mu\text{g m}^{-3} \text{ day}^{-1}$ ) and nocturnal  $\text{N}_2\text{O}_5$  uptake ( $15.6 \mu\text{g m}^{-3} \text{ day}^{-1}$ ) were the major nitrate  
496 formation pathways, which contributed 56% and 44% to the surface total nitrate  
497 production, respectively. Therefore, the importance of residual layer contribution to the  
498 surface nitrate can vary significantly and should be comprehensively evaluated in  
499 different environments. In addition, the nitrate contributions to the surface  
500 concentrations and boundary layer column concentrations can also be different in  
501 different regions, which should be clarified and distinguished in future studies.

502 In summary, the  $\text{N}_2\text{O}_5$  uptake reaction was active in the residual layer both at urban  
503 and suburban sites, the downward transport from the residual layer was a significant  
504 contributor to surface nitrate at the urban site, but not at the suburban site. This is  
505 attributable to the titration of the  $\text{NO}_3$  radical and ozone by fresh NO emissions during  
506 the stagnant boundary layer at the urban site, resulting in the large difference of nitrate  
507 production between the residual and nocturnal boundary layers. In contrast, at the  
508 suburban site, lower NO emissions favored  $\text{NO}_3$  production and heterogeneous uptake  
509 of  $\text{N}_2\text{O}_5$  both in the nocturnal boundary layer and the residual layer. The horizontal  
510 transport in the residual layer from nocturnal jets may contribute to the different nitrate  
511 production at urban and suburban sites, which has been discussed in the research of  
512 Chow et al. (2006) and Brown et al. (2006). Due to the limitation of box model, this  
513 issue could be studied by the chemistry transport model in further research.



### 514 **3.3 Control of NO<sub>x</sub> and VOCs as mitigation strategies of nitrate**

515 Overall, the contributions of nitrate from the three major pathways, all involving  
516 NO<sub>x</sub> and ozone, suggest that nitrate formation depends not only on the reactions of NO<sub>x</sub>  
517 but also is closely associated with the VOCs-NO<sub>x</sub>-O<sub>3</sub> chemistry. Therefore, the  
518 influence of both NO<sub>x</sub> and VOCs reduction on nitrate production should be considered  
519 in formulating policies to control aerosol pollution.

520 In this study, we adopted the widely used EKMA approach, generally used for  
521 ozone sensitivity analysis (Edwards et al., 2014;Mazzuca et al., 2016;Xue et al.,  
522 2014b;Wang et al., 2015) to investigate the response of nitrate formation in changing  
523 emissions of VOCs and NO<sub>x</sub>. The dependence of simulated nitrate concentrations with  
524 changing of VOCs and NO<sub>x</sub> concentration allow to construct isopleths of nitrate and  
525 ozone production at the GIG and Heshan sites, as displayed in Fig. 10. The production  
526 of nitrate and ozone were in the VOCs-limited regime at the GIG site, and in the  
527 transition regime at the Heshan site, where nitrate and ozone are sensitive to both VOCs  
528 and NO<sub>x</sub> reduction. As shown in Fig. 11, the reduction of NO<sub>x</sub> emissions from 0 ~ 70%  
529 would increase nitrate and ozone concentrations at the GIG site, but decrease those  
530 concentrations at the Heshan site. The decrease in VOCs concentrations would decrease  
531 nitrate and ozone concentrations at both sites. These results suggest that control of  
532 VOCs emissions will efficiently reduce nitrate and ozone production in both urban and  
533 suburban areas, but control of NO<sub>x</sub> emissions will give different responses between  
534 urban and suburban area for both ozone and nitrate. Fig. 11 show that the nitrate  
535 sensitivity to the reduction of VOCs and NO<sub>x</sub> emissions was identical to the response  
536 of ozone at both sites. These results demonstrate the possibility of synergetic control  
537 for nitrate and ozone at both urban and suburban sites through VOCs control.

538 The accuracy of the isopleth plots in Fig. 10 depends on several variables and  
539 parameters included in the box model. Figs S13 ~14 show the results of simulation  
540 experiments on the dependence of the isopleths upon changing various  
541 parameterization for estimating HONO concentrations, N<sub>2</sub>O<sub>5</sub> uptake coefficient, and  
542 ClNO<sub>2</sub> yields as described in Text S4. The sensitivity regime of nitrate and ozone did  
543 not change, although the peak concentrations of ozone and nitrate did change, which  
544 supports the reliability of the results discussed above.

545 As nitrate and ozone exhibit similar sensitivity to the reduction of NO<sub>x</sub> and VOCs,  
546 different VOCs/NO<sub>x</sub> ratios may point to different control strategies. In the cases of the

547 Heshan and GIG sites, the reduction of  $\text{NO}_x$  can adequately control nitrate production  
548 with a VOCs/ $\text{NO}_x$  ratio of 1.8 at the Heshan site, while a contrary result can be found  
549 at the GIG site (with a VOCs/ $\text{NO}_x$  ratio of 0.8) with a less than 70% reduction of  $\text{NO}_x$   
550 emission. The simulated results at the GIG site agree well with those reported in the  
551 urban areas of Shanghai in China (Dong et al., 2014) and the Salt Lake City and San  
552 Joaquin Valley in the US (Betty and Christian, 2001;Womack et al., 2019), which all  
553 emphasized the decrease of nitrate production with the reduction of VOCs emissions,  
554 and the enhanced nitrate production with  $\text{NO}_x$  reduction. The results at the Heshan site  
555 were consistent with the simulations at the suburban site of northern China, where a  
556 higher VOCs/ $\text{NO}_x$  ratio was found (Wen et al., 2018;Lu et al., 2019). The synergetic  
557 reduction of  $\text{NO}_x$  and VOCs is necessary to effectively mitigate the nitrate production  
558 in consideration of the different VOCs/ $\text{NO}_x$  ratios in the urban and suburban areas.

559 The above discussions revealed that direct reduction of  $\text{NO}_x$  may not lead to a  
560 decrease in nitrate production. Meanwhile, the reduction of VOCs is effective to  
561 mitigate nitrate production, though they were not the direct precursors of nitrate. To  
562 illustrate these findings, the impacts of changing VOCs and  $\text{NO}_x$  on the production rate  
563 of the OH radical, and the rate of OH plus  $\text{NO}_2$ , and the  $\text{N}_2\text{O}_5$  uptake reaction were  
564 evaluated. During daytime nitrate production involves OH production and its  
565 subsequent reaction with  $\text{NO}_2$ . As shown in Fig. 12, the  $\text{NO}_x$ -saturated condition at the  
566 GIG site provided sufficient  $\text{NO}_2$  to quench the OH radical during daytime. A less than  
567 70%reduction of  $\text{NO}_x$  will increase ozone production and thereby drive more  
568 production of OH, leading to increase in the OH and  $\text{NO}_2$  reaction rates. When  $\text{NO}_x$  is  
569 lower than 30% of the base case emissions, ozone production would decrease and lead  
570 to the decrease of OH production and its reaction with  $\text{NO}_2$ , which in turn bring about  
571 a decrease in nitrate production. In contrast, at the Heshan site, the base case  $\text{NO}_x$   
572 concentrations are lower, giving a production rate of OH that is already sensitive to  
573 both  $\text{NO}_x$  and VOCs reductions. The model results indicates that further emission  
574 reductions in both  $\text{NO}_x$  and VOCs will simultaneously mitigate the production of nitrate  
575 and ozone.

576 During nighttime, the initial ozone concentration participated the nocturnal  
577 chemistry increased/decreased with the reduction of  $\text{NO}_x$  at the GIG/Heshan site. In  
578 addition, the decrease in  $\text{NO}_x$  will reduce the titration effect of NO on  $\text{NO}_3$  radical and  
579 ozone at the GIG site, which enhances production of  $\text{N}_2\text{O}_5$  and promotes nitrate  
580 production in both the nocturnal boundary layer and the residual layer (Fig.13).

581 However, at the Heshan site, the reduction of  $\text{NO}_x$  cuts down the sources of  $\text{NO}_2$  and  
582  $\text{NO}_3$ , decreasing the formation of  $\text{N}_2\text{O}_5$  and thus its heterogeneous uptake to produce  
583 nitrate. The reduction of VOCs decreases ozone formation during daytime, thus  
584 attenuating the nocturnal formation of  $\text{NO}_3$ ,  $\text{N}_2\text{O}_5$  and nitrate at both the GIG and  
585 Heshan sites.

586 In summary, nitrate and ozone show similar responses to the reduction of  $\text{NO}_x$  and  
587 VOCs for both daytime and nighttime chemical processes, as the result of the coupling  
588 between the formation reactions of ozone and nitrate. The results of this study  
589 emphasize the complex effects of reductions of  $\text{NO}_x$  emissions on nitrate concentrations  
590 in the urban and suburban areas. In addition, the reduction of VOCs emissions would  
591 be effective in the concurrent mitigation of ozone and nitrate, suggesting that the  
592 reduction of VOCs at present is an effective method for the synergistic control of ozone  
593 and  $\text{PM}_{2.5}$  at present. As there are limitations of box modeling, a comprehensive three-  
594 dimensional model assessment is needed on a regional scale.

## 595 **4 Conclusions**

596 In this study, we use an observation-constrained box model to explore the nitrate  
597 formation pathways and implications for nitrate mitigation strategies at urban and  
598 suburban sites. At both sites, the mass fraction of nitrate in  $\text{PM}_1$  increased as the  
599 absolute  $\text{PM}_1$  levels increased (from 10% to 33% at the urban site and from 10% to 20%  
600 at the suburban site), suggesting the important role played by nitrate in increasing  
601 particle concentrations in the PRD.

602 Both  $\text{HNO}_3$  and  $\text{NH}_3$  are important precursors for nitrate formation. Combined  
603 with the ISORROPIA II thermodynamic model, the reduction of  $\text{NH}_3$  is effective for  
604 the nitrate reduction by affecting the partitioning process of nitrate at both GIG and  
605 Heshan site. The box model simulations demonstrate that chemical reactions in the  
606 daytime and at night both contributed significantly to formation of nitrate in the  
607 boundary layer at the two sites, with nighttime contributions of 58% at the urban site  
608 and 35% at the suburban site. However, nighttime reactions predominately occurred  
609 aloft in the residual layer at the urban site and downward transport from the residual  
610 layer in the morning are important source (53%) for surface nitrate at the urban site,  
611 whereas similar amounts of nitrate were produced in the nocturnal boundary layer and  
612 residual layer at the suburban site, which results in little downward transport of nitrate  
613 from the residual layer to the ground at this region. The spatial differences of nocturnal

614 reactions and the different contributions from downward transport of the residual layer  
615 to surface nitrate at urban and suburban sites were attributed to different fresh emissions  
616 and concentration levels of  $\text{NO}_x$  at the two sites during the night time, suggesting that  
617 nitrate production under different  $\text{NO}_x$  conditions should be explored to better  
618 understand the its formation pathways.

619 The non-linear relationships between nitrate and  $\text{NO}_x$ , VOCs was developed to  
620 investigate the nitrate mitigation strategies. The simulations demonstrated that the  
621 formation processes of both nitrate and ozone were in the VOCs-limited region at the  
622 urban site and in the transition region at the suburban site. The same sensitivity regimes  
623 of nitrate and ozone at two sites was caused by the similar chemical processes that  
624 account to produce nitrate and ozone. These results suggest that control of VOCs  
625 emissions would effectively mitigate nitrate in both urban and suburban areas.

626 Overall, the formation processes of nitrate are systematically investigated in both  
627 urban and suburban areas in this study, which provides the opportunity to identify  
628 different influencing factors of nitrate production in different environments and offers  
629 insights into the comprehensive mitigation of nitrate pollution in regional scale.  $\text{NO}_x$   
630 emission controls alone might not be an effective strategy for reducing the nitrate  
631 production, while the reduction of VOCs emissions would take effect in the concurrent  
632 mitigation of ozone and nitrate. Thus, an emission control policy focusing on VOCs  
633 will be an effective means for the synergistic control of ozone and  $\text{PM}_{2.5}$  at present. In  
634 the long-term, multi-pollutant control should be implemented to achieve better control  
635 strategies for ozone and  $\text{PM}_{2.5}$ . As the result of limitation for the 0-D box model, vertical  
636 transport and horizontal transport cannot be considered explicitly in this study. Given  
637 the limitations of the box model, three-dimensional models should be used to further  
638 investigate the synergistic control of ozone and particles on the regional scale.

### 639 **Data availability**

640 The observational data used in this study are available from corresponding authors  
641 upon request (byuan@jnu.edu.cn)

### 642 **Author contributions**

643 BY and MS designed the research. SXY, YWP, SH, WC, WWH, CLP, CMW,  
644 ZLW, TGL, EZ, MFC, XBL, SHW, CHW, WWJ, CSY, WS and PC contributed to data  
645 collection. SXY performed the data analysis, with contributions from JZ, DD. Parrish,

646 XJH, CCL, XYY, YS, HCW, DHC, XMW, ZYZ, JYZ and XMW. SXY and BY  
647 prepared the manuscript with contributions from the other authors. All the authors  
648 reviewed the manuscript.

### 649 **Competing interests**

650 The authors declare that they have no known competing financial interests or personal  
651 relationships that could have appeared to influence the work reported in this paper.

### 652 **Acknowledgments**

653 This work was supported by the National Key R&D Plan of China (grant No.  
654 2019YFE0106300, 2018YFC0213904, 2016YFC0202206), the National Natural  
655 Science Foundation of China (grant No. 41877302), the National Natural Science  
656 Foundation of China (grant No. 41905111), Guangdong Natural Science Funds for  
657 Distinguished Young Scholar (grant No. 2018B030306037), Key-Area Research and  
658 Development Program of Guangdong Province (grant No. 2019B110206001),  
659 Guangdong Soft Science Research Program (2019B101001005), and Guangdong  
660 Innovative and Entrepreneurial Research Team Program (grant No. 2016ZT06N263).  
661 This work was also supported by Special Fund Project for Science and Technology  
662 Innovation Strategy of Guangdong Province (Grant No.2019B121205004).

### 663 **References**

664 Anderson, D. C., Nicely, J. M., Wolfe, G. M., Hanisco, T. F., Salawitch, R. J., Canty, T. P.,  
665 Dickerson, R. R., Apel, E. C., Baidar, S., Bannan, T. J., Blake, N. J., Chen, D., Dix, B.,  
666 Fernandez, R. P., Hall, S. R., Hornbrook, R. S., Gregory Huey, L., Josse, B., Jöckel, P.,  
667 Kinnison, D. E., Koenig, T. K., Le Breton, M., Marécal, V., Morgenstern, O., Oman, L. D.,  
668 Pan, L. L., Percival, C., Plummer, D., Revell, L. E., Rozanov, E., Saiz-Lopez, A., Stenke, A.,  
669 Sudo, K., Tilmes, S., Ullmann, K., Volkamer, R., Weinheimer, A. J., and Zeng, G.:  
670 Formaldehyde in the Tropical Western Pacific: Chemical Sources and Sinks, Convective  
671 Transport, and Representation in CAM-Chem and the CCM1 Models, *Journal of Geophysical*  
672 *Research: Atmospheres*, 122, 11,201-211,226, <https://doi.org/10.1002/2016JD026121>, 2017.  
673 Baasandorj, M., Hoch, S. W., Bares, R., Lin, J. C., Brown, S. S., Millet, D. B., Martin, R.,  
674 Kelly, K., Zarzana, K. J., Whiteman, C. D., Dube, W. P., Tonnesen, G., Jaramillo, I. C., and  
675 Sohl, J.: Coupling between Chemical and Meteorological Processes under Persistent Cold-Air  
676 Pool Conditions: Evolution of Wintertime PM<sub>2.5</sub> Pollution Events and N<sub>2</sub>O<sub>5</sub> Observations in  
677 Utah's Salt Lake Valley, *Environmental Science & Technology*, 51, 5941-5950,

678 10.1021/acs.est.6b06603, 2017.

679 Bertram, T., and Thornton, J.: Toward a general parameterization of N<sub>2</sub>O<sub>5</sub> reactivity on  
680 aqueous particles: The competing effects of particle liquid water, nitrate and chloride,  
681 Atmospheric Chemistry and Physics Discussions, 9, 15181-15214, 2009.

682 Betty, P., and Christian: Sensitivity of particulate matter nitrate formation to precursor  
683 emissions in the California San Joaquin Valley, Environmental Science & Technology, 35,  
684 2979-2987, 2001.

685 Bian, H., Chin, M., Hauglustaine, D. A., Schulz, M., Myhre, G., Bauer, S. E., Lund, M. T.,  
686 Karydis, V. A., Kucsera, T. L., Pan, X., Pozzer, A., Skeie, R. B., Steenrod, S. D., Sudo, K.,  
687 Tsigaridis, K., Tsimpidi, A. P., and Tsyro, S. G.: Investigation of global particulate nitrate  
688 from the AeroCom phase III experiment, Atmos. Chem. Phys., 17, 12911-12940,  
689 10.5194/acp-17-12911-2017, 2017.

690 Bloss, C., Wagner, V., Jenkin, M. E., Volkamer, R., Bloss, W. J., Lee, J. D., Heard, D. E.,  
691 Wirtz, K., Martin-Reviejo, M., Rea, G., Wenger, J. C., and Pilling, M. J.: Development of a  
692 detailed chemical mechanism (MCMv3.1) for the atmospheric oxidation of aromatic  
693 hydrocarbons, Atmos. Chem. Phys., 5, 641-664, 10.5194/acp-5-641-2005, 2005.

694 Brown, S. G., Hyslop, N. P., Roberts, P. T., McCarthy, M. C., and Lurmann, F. W.: Wintertime  
695 Vertical Variations in Particulate Matter (PM) and Precursor Concentrations in the San  
696 Joaquin Valley during the California Regional Coarse PM/Fine PM Air Quality Study, Journal  
697 of the Air & Waste Management Association, 56, 1267-1277,  
698 10.1080/10473289.2006.10464583, 2006.

699 Brown, S. S., Stark, H., Ryerson, T. B., Williams, E. J., Nicks Jr., D. K., Trainer, M.,  
700 Fehsenfeld, F. C., and Ravishankara, A. R.: Nitrogen oxides in the nocturnal boundary layer:  
701 Simultaneous in situ measurements of NO<sub>3</sub>, N<sub>2</sub>O<sub>5</sub>, NO<sub>2</sub>, NO, and O<sub>3</sub>, Journal of  
702 Geophysical Research: Atmospheres, 108, 10.1029/2002jd002917, 2003.

703 Chen, W., Ye, Y., Hu, W., Zhou, H., Pan, T., Wang, Y., Song, W., Song, Q., Ye, C., Wang, C.,  
704 Wang, B., Huang, S., Yuan, B., Zhu, M., Lian, X., Zhang, G., Bi, X., Jiang, F., Liu, J.,  
705 Canonaco, F., Prevot, A. S. H., Shao, M., and Wang, X.: Real-time characterization of aerosol  
706 compositions, sources and aging processes in Guangzhou during PRIDE-GBA 2018  
707 campaign, Journal of Geophysical Research: Atmospheres, n/a, e2021JD035114,  
708 <https://doi.org/10.1029/2021JD035114>, 2021.

709 Chen, X., Wang, H., Lu, K., Li, C., Zhai, T., Tan, Z., Ma, X., Yang, X., Liu, Y., Chen, S.,  
710 Dong, H., Li, X., Wu, Z., Hu, M., Zeng, L., and Zhang, Y.: Field Determination of Nitrate  
711 Formation Pathway in Winter Beijing, Environmental Science & Technology,  
712 10.1021/acs.est.0c00972, 2020.

713 Chow, J. C., Chen, L. W. A., Watson, J. G., Lowenthal, D. H., Magliano, K. A., Turkiewicz,  
714 K., and Lehrman, D. E.: PM<sub>2.5</sub> chemical composition and spatiotemporal variability during

715 the California Regional PM<sub>10</sub>/PM<sub>2.5</sub> Air Quality Study (CRPAQS), *Journal of Geophysical*  
716 *Research: Atmospheres*, 111, 2006.

717 Curci, G., Ferrero, L., Tuccella, P., Barnaba, F., Angelini, F., Bolzacchini, E., Carbone, C., Der  
718 Gon, H. A. C. D. V., Facchini, M. C., and Gobbi, G. P.: How much is particulate matter near  
719 the ground influenced by upper-level processes within and above the PBL? A summertime  
720 case study in Milan (Italy) evidences the distinctive role of nitrate, *Atmospheric Chemistry*  
721 *and Physics*, 15, 2629-2649, 2015.

722 D'Ambro, E. L., Møller, K. H., Lopez-Hilfiker, F. D., Schobesberger, S., Liu, J., Shilling, J.  
723 E., Lee, B. H., Kjaergaard, H. G., and Thornton, J. A.: Isomerization of Second-Generation  
724 Isoprene Peroxy Radicals: Epoxide Formation and Implications for Secondary Organic  
725 Aerosol Yields, *Environmental Science & Technology*, 51, 4978-4987,  
726 10.1021/acs.est.7b00460, 2017.

727 Decker, Z. C. J., Zarzana, K. J., Coggon, M., Min, K.-E., Pollack, I., Ryerson, T. B., Peischl,  
728 J., Edwards, P., Dubé, W. P., Markovic, M. Z., Roberts, J. M., Veres, P. R., Graus, M.,  
729 Warneke, C., de Gouw, J., Hatch, L. E., Barsanti, K. C., and Brown, S. S.: Nighttime  
730 Chemical Transformation in Biomass Burning Plumes: A Box Model Analysis Initialized with  
731 Aircraft Observations, *Environmental Science & Technology*, 53, 2529-2538,  
732 10.1021/acs.est.8b05359, 2019.

733 Dong, H. B., Zeng, L. M., Hu, M., Wu, Y. S., Zhang, Y. H., Slanina, J., Zheng, M., Wang, Z.  
734 F., and Jansen, R.: Technical Note: The application of an improved gas and aerosol collector  
735 for ambient air pollutants in China, *Atmos. Chem. Phys.*, 12, 10519-10533, 10.5194/acp-12-  
736 10519-2012, 2012.

737 Dong, X., Li, J., Fu, J. S., Gao, Y., Huang, K., and Zhuang, G.: Inorganic aerosols responses  
738 to emission changes in Yangtze River Delta, China, *Science of The Total Environment*, 481,  
739 522-532, 2014.

740 Edwards, P., Aikin, K. C., Dube, W. P., Fry, J. L., Gilman, J. B., De Gouw, J. A., Graus, M.,  
741 Hanisco, T. F., Holloway, J. S., and Hubler, G.: Transition from high- to low-NO<sub>x</sub> control of  
742 night-time oxidation in the southeastern US, *Nature Geoscience*, 10, 490-495, 2017.

743 Edwards, P. M., Brown, S. S., Roberts, J. M., Ahmadov, R., Banta, R. M., deGouw, J. A.,  
744 Dubé, W. P., Field, R. A., Flynn, J. H., Gilman, J. B., Graus, M., Helmig, D., Koss, A.,  
745 Langford, A. O., Lefer, B. L., Lerner, B. M., Li, R., Li, S.-M., McKeen, S. A., Murphy, S. M.,  
746 Parrish, D. D., Senff, C. J., Soltis, J., Stutz, J., Sweeney, C., Thompson, C. R., Trainer, M. K.,  
747 Tsai, C., Veres, P. R., Washenfelder, R. A., Warneke, C., Wild, R. J., Young, C. J., Yuan, B.,  
748 and Zamora, R.: High winter ozone pollution from carbonyl photolysis in an oil and gas  
749 basin, *Nature*, 514, 351, 10.1038/nature13767, 2014.

750 Ervens, B., George, C., Williams, J. E., Buxton, G. V., Salmon, G. A., Bydder, M., Wilkinson,  
751 F., Dentener, F., Mirabel, P., Wolke, R., and Herrmann, H.: CAPRAM 2.4 (MODAC

752 mechanism): An extended and condensed tropospheric aqueous phase mechanism and its  
753 application, *Journal of Geophysical Research: Atmospheres*, 108, 10.1029/2002JD002202,  
754 2003.

755 Fountoukis, C., and Nenes, A.: ISORROPIA II: a computationally efficient thermodynamic  
756 equilibrium model for  
757  $K^+ - Ca^{2+} - Mg^{2+} - NH_4^+$   
758  $Na^+ - SO_4^{2-}$   
759  $- NO_3^- - Cl^- - H_2O$   
760 aerosols, *Atmos. Chem. Phys.*, 7, 4639-4659, 10.5194/acp-7-4639-2007, 2007.

761 Franchin, A., Fibiger, D. L., Goldberger, L., McDuffie, E. E., Moravek, A., Womack, C. C.,  
762 Crosman, E. T., Docherty, K. S., Dube, W. P., Hoch, S. W., Lee, B. H., Long, R., Murphy, J.  
763 G., Thornton, J. A., Brown, S. S., Baasandorj, M., and Middlebrook, A. M.: Airborne and  
764 ground-based observations of ammonium-nitrate-dominated aerosols in a shallow boundary  
765 layer during intense winter pollution episodes in northern Utah, *Atmos. Chem. Phys.*, 18,  
766 17259-17276, 10.5194/acp-18-17259-2018, 2018.

767 Fu, X., Wang, T., Gao, J., Wang, P., Liu, Y., Wang, S., Zhao, B., and Xue, L.: Persistent Heavy  
768 Winter Nitrate Pollution Driven by Increased Photochemical Oxidants in Northern China,  
769 *Environmental Science & Technology*, 54, 3881-3889, 10.1021/acs.est.9b07248, 2020.

770 Gen, M., Zhang, R., Huang, D. D., Li, Y., and Chan, C. K.: Heterogeneous SO<sub>2</sub> Oxidation in  
771 Sulfate Formation by Photolysis of Particulate Nitrate, *Environmental Science & Technology*  
772 *Letters*, 6, 86-91, 10.1021/acs.estlett.8b00681, 2019.

773 Geyer, A., and Stutz, J.: Vertical profiles of NO<sub>3</sub>, N<sub>2</sub>O<sub>5</sub>, O<sub>3</sub>, and NO<sub>x</sub> in the nocturnal  
774 boundary layer: 2. Model studies on the altitude dependence of composition and chemistry,  
775 *Journal of Geophysical Research*, 109, 2004.

776 Griffith, S. M., Huang, X. H. H., Louie, P. K. K., and Yu, J. Z.: Characterizing the  
777 thermodynamic and chemical composition factors controlling PM<sub>2.5</sub> nitrate: Insights gained  
778 from two years of online measurements in Hong Kong, *Atmospheric Environment*, 122, 864-  
779 875, <https://doi.org/10.1016/j.atmosenv.2015.02.009>, 2015.

780 Guo, H., Otjes, R., Schlag, P., Kiendler-Scharr, A., Nenes, A., and Weber, R. J.: Effectiveness  
781 of ammonia reduction on control of fine particle nitrate, *Atmos. Chem. Phys.*, 18, 12241-  
782 12256, 10.5194/acp-18-12241-2018, 2018.

783 Hou, X., Chan, C., Dong, G., and Yim, S.: Impacts of transboundary air pollution and local  
784 emissions on PM<sub>2.5</sub> pollution in the Pearl River Delta region of China and the public health,  
785 and the policy implications, *Environmental Research Letters*, 14, 034005, 2019.

786 Hu, W., Hu, M., Hu, W., Jimenez, J. L., Yuan, B., Chen, W., Wang, M., Wu, Y., Chen, C.,  
787 Wang, Z., Peng, J., Zeng, L., and Shao, M.: Chemical composition, sources, and aging  
788 process of submicron aerosols in Beijing: Contrast between summer and winter, *Journal of*



789 Geophysical Research: Atmospheres, 121, 1955-1977,  
790 <https://doi.org/10.1002/2015JD024020>, 2016.

791 Jacob, D. J.: Heterogeneous chemistry and tropospheric ozone, Atmospheric Environment,  
792 34, 2131-2159, [https://doi.org/10.1016/S1352-2310\(99\)00462-8](https://doi.org/10.1016/S1352-2310(99)00462-8), 2000.

793 Jenkin, M. E., Saunders, S. M., Wagner, V., and Pilling, M. J.: Protocol for the development  
794 of the Master Chemical Mechanism, MCM v3 (Part B): tropospheric degradation of aromatic  
795 volatile organic compounds, Atmos. Chem. Phys., 3, 181-193, 10.5194/acp-3-181-2003,  
796 2003.

797 Lawal, A. S., Guan, X., Liu, C., Henneman, L. R. F., Vasilakos, P., Bhogineni, V., Weber, R.  
798 J., Nenes, A., and Russell, A. G.: Linked Response of Aerosol Acidity and Ammonia to SO<sub>2</sub>  
799 and NO<sub>x</sub> Emissions Reductions in the United States, Environmental Science & Technology,  
800 52, 9861-9873, 10.1021/acs.est.8b00711, 2018.

801 Li, H., Zhang, Q., Zheng, B., Chen, C., Wu, N., Guo, H., Zhang, Y., Zheng, Y., Li, X., and He,  
802 K.: Nitrate-driven urban haze pollution during summertime over the North China Plain,  
803 Atmos. Chem. Phys., 18, 5293-5306, 10.5194/acp-18-5293-2018, 2018.

804 Li, L., Lu, C., Chan, P.-W., Zhang, X., Yang, H.-L., Lan, Z.-J., Zhang, W.-H., Liu, Y.-W., Pan,  
805 L., and Zhang, L.: Tower observed vertical distribution of PM<sub>2.5</sub>, O<sub>3</sub> and NO<sub>x</sub> in the Pearl  
806 River Delta, Atmospheric Environment, 220, 117083,  
807 <https://doi.org/10.1016/j.atmosenv.2019.117083>, 2020.

808 Li, S. M., Anlauf, K., and Wiebe, H.: Heterogeneous nighttime production and deposition of  
809 particle nitrate at a rural site in North America during summer 1988, Journal of Geophysical  
810 Research: Atmospheres, 98, 5139-5157, 1993.

811 Lin, Y. C., Zhang, Y. L., Fan, M. Y., and Bao, M.: Heterogeneous formation of particulate  
812 nitrate under ammonium-rich regimes during the high-PM<sub>2.5</sub> events in Nanjing, China,  
813 Atmos. Chem. Phys., 20, 3999-4011, 10.5194/acp-20-3999-2020, 2020.

814 Liu, J., Ren, C., Huang, X., Nie, W., Wang, J., Sun, P., Chi, X., and Ding, A.: Increased  
815 Aerosol Extinction Efficiency Hinders Visibility Improvement in Eastern China, Geophysical  
816 Research Letters, 47, e2020GL090167, <https://doi.org/10.1029/2020GL090167>, 2020.

817 Liu, J., Liu, Z., Ma, Z., Yang, S., Yao, D., Zhao, S., Hu, B., Tang, G., Sun, J., Cheng, M., Xu,  
818 Z., and Wang, Y.: Detailed budget analysis of HONO in Beijing, China: Implication on  
819 atmosphere oxidation capacity in polluted megacity, Atmospheric Environment, 244, 117957,  
820 <https://doi.org/10.1016/j.atmosenv.2020.117957>, 2021.

821 Liu, M., Huang, X., Song, Y., Tang, J., Cao, J., Zhang, X., Zhang, Q., Wang, S., Xu, T., Kang,  
822 L., Cai, X., Zhang, H., Yang, F., Wang, H., Yu, J. Z., Lau, A. K. H., He, L., Huang, X., Duan,  
823 L., Ding, A., Xue, L., Gao, J., Liu, B., and Zhu, T.: Ammonia emission control in China  
824 would mitigate haze pollution and nitrogen deposition, but worsen acid rain, Proceedings of  
825 the National Academy of Sciences, 116, 7760, 10.1073/pnas.1814880116, 2019a.

826 Liu, X., Sun, K., Qu, Y., Hu, M., Sun, Y., Zhang, F., and Zhang, Y.: Secondary formation of  
827 sulfate and nitrate during a haze episode in megacity Beijing, China, *Aerosol Air Qual. Res.*,  
828 15, 2246-2257, 2015.

829 Liu, X., Lyu, X., Wang, Y., Jiang, F., and Guo, H.: Intercomparison of O<sub>3</sub> formation and  
830 radical chemistry in the past decade at a suburban site in Hong Kong, *Atmos. Chem. Phys.*,  
831 19, 5127-5145, 10.5194/acp-19-5127-2019, 2019b.

832 Lou, S., Holland, F., Rohrer, F., Lu, K., Bohn, B., Brauers, T., Chang, C., Fuchs, H., Häseler,  
833 R., and Kita, K.: Atmospheric OH reactivities in the Pearl River Delta-China in summer 2006:  
834 measurement and model results, *Atmospheric Chemistry and Physics*, 10, 11243, 2010.

835 Lu, K., Rohrer, F., Holland, F., Fuchs, H., Bohn, B., Brauers, T., Chang, C., Häseler, R., Hu,  
836 M., and Kita, K.: Observation and modelling of OH and HO<sub>2</sub> concentrations in the Pearl  
837 River Delta 2006: a missing OH source in a VOC rich atmosphere, *Atmospheric chemistry  
838 and physics*, 12, 1541, 2012.

839 Lu, K., Fuchs, H., Hofzumahaus, A., Tan, Z., Wang, H., Zhang, L., Schmitt, S. H., Rohrer, F.,  
840 Bohn, B., Broch, S., Dong, H., Gkatzelis, G. I., Hohaus, T., Holland, F., Li, X., Liu, Y., Liu,  
841 Y., Ma, X., Novelli, A., Schlag, P., Shao, M., Wu, Y., Wu, Z., Zeng, L., Hu, M., Kiendler-  
842 Schar, A., Wahner, A., and Zhang, Y.: Fast Photochemistry in Wintertime Haze:  
843 Consequences for Pollution Mitigation Strategies, *Environmental Science & Technology*,  
844 10.1021/acs.est.9b02422, 2019.

845 Lu, K. D., Hofzumahaus, A., Holland, F., Bohn, B., Brauers, T., Fuchs, H., Hu, M., seler, R.  
846 H., Kita, K., Kondo, Y., Li, X., Lou, S. R., Oebel, A., Shao, M., Zeng, L. M., Wahner, A., Zhu,  
847 T., Zhang, Y. H., and Rohrer, F.: Missing OH source in a suburban environment near Beijing:  
848 observed and modelled OH and HO<sub>2</sub> concentrations in summer 2006, *Atmospheric Chemistry  
849 and Physics (ACP) & Discussions (ACPD)*, 2013.

850 Lu, X., Chen, N., Wang, Y., Cao, W., Zhu, B., Yao, T., Fung, J. C. H., and Lau, A. K. H.:  
851 Radical budget and ozone chemistry during autumn in the atmosphere of an urban site in  
852 central China, *Journal of Geophysical Research: Atmospheres*, 122, 3672-3685,  
853 <https://doi.org/10.1002/2016JD025676>, 2017.

854 Lyu, X., Wang, N., Guo, H., Xue, L., Jiang, F., Zeren, Y., Cheng, H., Cai, Z., Han, L., and  
855 Zhou, Y.: Causes of a continuous summertime O<sub>3</sub> pollution event in Jinan, a central city in the  
856 North China Plain, *Atmos. Chem. Phys.*, 19, 3025-3042, 10.5194/acp-19-3025-2019, 2019.

857 Lyu, X. P., Zeng, L. W., Guo, H., Simpson, I. J., Ling, Z. H., Wang, Y., Murray, F., Louie, P.  
858 K. K., Saunders, S. M., Lam, S. H. M., and Blake, D. R.: Evaluation of the effectiveness of air  
859 pollution control measures in Hong Kong, *Environmental Pollution*, 220, 87-94,  
860 <https://doi.org/10.1016/j.envpol.2016.09.025>, 2017.

861 Mazzuca, G. M., Ren, X., Loughner, C. P., Estes, M., Crawford, J. H., Pickering, K. E.,  
862 Weinheimer, A. J., and Dickerson, R. R.: Ozone production and its sensitivity to NO<sub>x</sub> and

863 VOCs: results from the DISCOVER-AQ field experiment, Houston 2013, *Atmos. Chem.*  
864 *Phys.*, 13, 14463-14474, 2016.

865 McDuffie, E. E., Fibiger, D. L., Dubé, W. P., Lopez-Hilfiker, F., Lee, B. H., Thornton, J. A.,  
866 Shah, V., Jaeglé, L., Guo, H., Weber, R. J., Michael Reeves, J., Weinheimer, A. J., Schroder, J.  
867 C., Campuzano-Jost, P., Jimenez, J. L., Dibb, J. E., Veres, P., Ebben, C., Sparks, T. L.,  
868 Wooldridge, P. J., Cohen, R. C., Hornbrook, R. S., Apel, E. C., Campos, T., Hall, S. R.,  
869 Ullmann, K., and Brown, S. S.: Heterogeneous N<sub>2</sub>O<sub>5</sub> Uptake During Winter: Aircraft  
870 Measurements During the 2015 WINTER Campaign and Critical Evaluation of Current  
871 Parameterizations, *Journal of Geophysical Research: Atmospheres*, 123, 4345-4372,  
872 10.1002/2018JD028336, 2018a.

873 McDuffie, E. E., Fibiger, D. L., Dubé, W. P., Lopez Hilfiker, F., Lee, B. H., Jaeglé, L., Guo,  
874 H., Weber, R. J., Reeves, J. M., Weinheimer, A. J., Schroder, J. C., Campuzano-Jost, P.,  
875 Jimenez, J. L., Dibb, J. E., Veres, P., Ebben, C., Sparks, T. L., Wooldridge, P. J., Cohen, R. C.,  
876 Campos, T., Hall, S. R., Ullmann, K., Roberts, J. M., Thornton, J. A., and Brown, S. S.:  
877 ClNO<sub>2</sub> Yields From Aircraft Measurements During the 2015 WINTER Campaign and Critical  
878 Evaluation of the Current Parameterization, *Journal of Geophysical Research: Atmospheres*,  
879 123, 12,994-913,015, <https://doi.org/10.1029/2018JD029358>, 2018b.

880 McDuffie, E. E., Womack, C. C., Fibiger, D. L., Dube, W. P., Franchin, A., Middlebrook, A.  
881 M., Goldberger, L., Lee, B. H., Thornton, J. A., Moravek, A., Murphy, J. G., Baasandorj, M.,  
882 and Brown, S. S.: On the contribution of nocturnal heterogeneous reactive nitrogen chemistry  
883 to particulate matter formation during wintertime pollution events in Northern Utah, *Atmos.*  
884 *Chem. Phys.*, 19, 9287-9308, 10.5194/acp-19-9287-2019, 2019.

885 Mozurkewich, M.: The dissociation constant of ammonium nitrate and its dependence on  
886 temperature, relative humidity and particle size, *Atmospheric Environment. Part A. General*  
887 *Topics*, 27, 261-270, [https://doi.org/10.1016/0960-1686\(93\)90356-4](https://doi.org/10.1016/0960-1686(93)90356-4), 1993.

888 Nenes, A., Pandis, S. N., Weber, R. J., and Russell, A.: Aerosol pH and liquid water content  
889 determine when particulate matter is sensitive to ammonia and nitrate availability, *Atmos.*  
890 *Chem. Phys.*, 20, 3249-3258, 10.5194/acp-20-3249-2020, 2020.

891 Novak, G. A., and Bertram, T. H.: Reactive VOC Production from Photochemical and  
892 Heterogeneous Reactions Occurring at the Air–Ocean Interface, *Accounts of Chemical*  
893 *Research*, 53, 1014-1023, 10.1021/acs.accounts.0c00095, 2020.

894 Pathak, R. K., Wu, W. S., and Wang, T.: Summertime PM<sub>2.5</sub> ionic species in  
895 four major cities of China: nitrate formation in an ammonia-deficient atmosphere, *Atmos.*  
896 *Chem. Phys.*, 9, 1711-1722, 10.5194/acp-9-1711-2009, 2009.

897 Pathak, R. K., Wang, T., and Wu, W. S.: Nighttime enhancement of PM<sub>2.5</sub> nitrate in  
898 ammonia-poor atmospheric conditions in Beijing and Shanghai: Plausible contributions of  
899 heterogeneous hydrolysis of N<sub>2</sub>O<sub>5</sub> and HNO<sub>3</sub> partitioning, *Atmospheric Environment*, 45,

900 1183-1191, <https://doi.org/10.1016/j.atmosenv.2010.09.003>, 2011.

901 Prabhakar, G., Parworth, C. L., Zhang, X., Kim, H., Young, D. E., Beyersdorf, A. J., Ziemba,  
902 L. D., Nowak, J. B., Bertram, T. H., Faloon, I. C., Zhang, Q., and Cappa, C. D.:  
903 Observational assessment of the role of nocturnal residual-layer chemistry in determining  
904 daytime surface particulate nitrate concentrations, *Atmos. Chem. Phys.*, 17, 14747-14770,  
905 10.5194/acp-17-14747-2017, 2017.

906 Qin, Y. M., Tan, H. B., Li, Y. J., Schurman, M. I., Li, F., Canonaco, F., Prévôt, A. S. H., and  
907 Chan, C. K.: Impacts of traffic emissions on atmospheric particulate nitrate and organics at a  
908 downwind site on the periphery of Guangzhou, China, *Atmos. Chem. Phys.*, 17, 10245-  
909 10258, 10.5194/acp-17-10245-2017, 2017.

910 Riedel, T. P., Wolfe, G. M., Danas, K. T., Gilman, J. B., Kuster, W. C., Bon, D. M., Vlasenko,  
911 A., Li, S. M., Williams, E. J., Lerner, B. M., Veres, P. R., Roberts, J. M., Holloway, J. S.,  
912 Lefer, B., Brown, S. S., and Thornton, J. A.: An MCM modeling study of nitryl chloride  
913 (CINO<sub>2</sub>) impacts on oxidation, ozone production and nitrogen oxide partitioning  
914 in polluted continental outflow, *Atmos. Chem. Phys.*, 14, 3789-3800, 10.5194/acp-14-3789-  
915 2014, 2014.

916 Romer, P. S., Wooldridge, P. J., Crouse, J. D., Kim, M. J., Wennberg, P. O., Dibb, J. E.,  
917 Scheuer, E., Blake, D. R., Meinardi, S., Brosius, A. L., Thames, A. B., Miller, D. O., Brune,  
918 W. H., Hall, S. R., Ryerson, T. B., and Cohen, R. C.: Constraints on Aerosol Nitrate  
919 Photolysis as a Potential Source of HONO and NO<sub>x</sub>, *Environmental Science & Technology*,  
920 52, 13738-13746, 10.1021/acs.est.8b03861, 2018.

921 Saunders, S. M., Jenkin, M. E., Derwent, R. G., and Pilling, M. J.: Protocol for the  
922 development of the Master Chemical Mechanism, MCM v3 (Part A): tropospheric  
923 degradation of non-aromatic volatile organic compounds, *Atmos. Chem. Phys.*, 3, 161-180,  
924 10.5194/acp-3-161-2003, 2003.

925 Stelson, A. W., and Seinfeld, J. H.: Relative humidity and temperature dependence of the  
926 ammonium nitrate dissociation constant, *Atmospheric Environment* (1967), 16, 983-992,  
927 [https://doi.org/10.1016/0004-6981\(82\)90184-6](https://doi.org/10.1016/0004-6981(82)90184-6), 1982.

928 Su, T., Li, J., Tian, C., Zong, Z., Chen, D., and Zhang, G.: Source and formation of fine  
929 particulate nitrate in South China: Constrained by isotopic modeling and online trace gas  
930 analysis, *Atmospheric Environment*, 231, 117563,  
931 <https://doi.org/10.1016/j.atmosenv.2020.117563>, 2020.

932 Tan, Z., Lu, K., Jiang, M., Su, R., Dong, H., Zeng, L., Xie, S., Tan, Q., and Zhang, Y.:  
933 Exploring ozone pollution in Chengdu, southwestern China: A case study from radical  
934 chemistry to O<sub>3</sub>-VOC-NO<sub>x</sub> sensitivity, *Science of The Total Environment*, 636, 775-786,  
935 <https://doi.org/10.1016/j.scitotenv.2018.04.286>, 2018.

936 Tang, G., Wang, Y., Liu, Y., Wu, S., Huang, X., Yang, Y., Wang, Y., Ma, J., Bao, X., Liu, Z., Ji,

937 D., Li, T., Li, X., and Wang, Y.: Low particulate nitrate in the residual layer in autumn over  
938 the North China Plain, *Science of The Total Environment*, 782, 146845,  
939 <https://doi.org/10.1016/j.scitotenv.2021.146845>, 2021.

940 Tao, J., Zhang, Z., Tan, H., Zhang, L., Wu, Y., Sun, J., Che, H., Cao, J., Cheng, P., Chen, L.,  
941 and Zhang, R.: Observational evidence of cloud processes contributing to daytime elevated  
942 nitrate in an urban atmosphere, *Atmospheric Environment*, 186, 209-215,  
943 <https://doi.org/10.1016/j.atmosenv.2018.05.040>, 2018.

944 Tao, Y., Ye, X., Ma, Z., Xie, Y., Wang, R., Chen, J., Yang, X., and Jiang, S.: Insights into  
945 different nitrate formation mechanisms from seasonal variations of secondary inorganic  
946 aerosols in Shanghai, *Atmospheric Environment*, 145, 1-9,  
947 <https://doi.org/10.1016/j.atmosenv.2016.09.012>, 2016.

948 von Bobruzki, K., Braban, C. F., Famulari, D., Jones, S. K., Blackall, T., Smith, T. E. L.,  
949 Blom, M., Coe, H., Gallagher, M., Ghalaieny, M., McGillen, M. R., Percival, C. J.,  
950 Whitehead, J. D., Ellis, R., Murphy, J., Mohacsi, A., Pogany, A., Junninen, H., Rantanen, S.,  
951 Sutton, M. A., and Nemitz, E.: Field inter-comparison of eleven atmospheric ammonia  
952 measurement techniques, *Atmos. Meas. Tech.*, 3, 91-112, 10.5194/amt-3-91-2010, 2010.

953 Wang, C., Yuan, B., Wu, C., Wang, S., Qi, J., Wang, B., Wang, Z., Hu, W., Chen, W., Ye, C.,  
954 Wang, W., Sun, Y., Wang, C., Huang, S., Song, W., Wang, X., Yang, S., Zhang, S., Xu, W.,  
955 Ma, N., Zhang, Z., Jiang, B., Su, H., Cheng, Y., Wang, X., and Shao, M.: Measurements of  
956 higher alkanes using NO<sup>+</sup> chemical ionization in PTR-ToF-MS: important contributions of  
957 higher alkanes to secondary organic aerosols in China, *Atmos. Chem. Phys.*, 20, 14123-  
958 14138, 10.5194/acp-20-14123-2020, 2020a.

959 Wang, H., Lu, K., Chen, X., Zhu, Q., Chen, Q., Guo, S., Jiang, M., Li, X., Shang, D., Tan, Z.,  
960 Wu, Y., Wu, Z., Zou, Q., Zheng, Y., Zeng, L., Zhu, T., Hu, M., and Zhang, Y.: High N<sub>2</sub>O<sub>5</sub>  
961 Concentrations Observed in Urban Beijing: Implications of a Large Nitrate Formation  
962 Pathway, *Environmental Science & Technology Letters*, 4, 416-420,  
963 10.1021/acs.estlett.7b00341, 2017a.

964 Wang, H., Lu, K., Tan, Z., Sun, K., Li, X., Hu, M., Shao, M., Zeng, L., Zhu, T., and Zhang, Y.:  
965 Model simulation of NO<sub>3</sub>, N<sub>2</sub>O<sub>5</sub> and ClNO<sub>2</sub> at a rural site in Beijing during CAREBeijing-  
966 2006, *Atmospheric Research*, 196, 97-107, <https://doi.org/10.1016/j.atmosres.2017.06.013>,  
967 2017b.

968 Wang, H., Lu, K., Chen, X., Zhu, Q., Wu, Z., Wu, Y., and Sun, K.: Fast particulate nitrate  
969 formation via N<sub>2</sub>O<sub>5</sub> uptake aloft in winter in Beijing, *Atmos. Chem. Phys.*, 18, 10483-10495,  
970 10.5194/acp-18-10483-2018, 2018a.

971 Wang, H., Lu, K., Guo, S., Wu, Z., Shang, D., Tan, Z., Wang, Y., Le Breton, M., Lou, S.,  
972 Tang, M., Wu, Y., Zhu, W., Zheng, J., Zeng, L., Hallquist, M., Hu, M., and Zhang, Y.:  
973 Efficient N<sub>2</sub>O<sub>5</sub> uptake and NO<sub>3</sub> oxidation in the outflow of urban Beijing, *Atmos. Chem.*

974 Phys., 18, 9705-9721, 10.5194/acp-18-9705-2018, 2018b.

975 Wang, N., Guo, H., Jiang, F., Ling, Z. H., and Wang, T.: Simulation of ozone formation at  
976 different elevations in mountainous area of Hong Kong using WRF-CMAQ model, Science of  
977 The Total Environment, 505, 939-951, <https://doi.org/10.1016/j.scitotenv.2014.10.070>, 2015.

978 Wang, N., Lyu, X., Deng, X., Huang, X., Jiang, F., and Ding, A.: Aggravating O<sub>3</sub> pollution  
979 due to NO<sub>x</sub> emission control in eastern China, Science of The Total Environment, 677, 732-  
980 744, <https://doi.org/10.1016/j.scitotenv.2019.04.388>, 2019.

981 Wang, Y., Zhang, Y., Hao, J., and Luo, M.: Seasonal and spatial variability of surface ozone  
982 over China: contributions from background and domestic pollution, Atmos. Chem. Phys., 11,  
983 3511-3525, 10.5194/acp-11-3511-2011, 2011.

984 Wang, Z., Yuan, B., Ye, C., Roberts, J., Wisthaler, A., Lin, Y., Li, T., Wu, C., Peng, Y., Wang,  
985 C., Wang, S., Yang, S., Wang, B., Qi, J., Wang, C., Song, W., Hu, W., Wang, X., Xu, W., Ma,  
986 N., Kuang, Y., Tao, J., Zhang, Z., Su, H., Cheng, Y., Wang, X., and Shao, M.: High  
987 Concentrations of Atmospheric Isocyanic Acid (HNCO) Produced from Secondary Sources in  
988 China, Environmental Science & Technology, 54, 11818-11826, 10.1021/acs.est.0c02843,  
989 2020b.

990 Watson, J. G.: Visibility: Science and Regulation, Journal of The Air & Waste Management  
991 Association, 52, 973-999, 2002.

992 Wen, L., Chen, J., Yang, L., Wang, X., Caihong, X., Sui, X., Yao, L., Zhu, Y., Zhang, J., Zhu,  
993 T., and Wang, W.: Enhanced formation of fine particulate nitrate at a rural site on the North  
994 China Plain in summer: The important roles of ammonia and ozone, Atmospheric  
995 Environment, 101, 294-302, <https://doi.org/10.1016/j.atmosenv.2014.11.037>, 2015.

996 Wen, L., Xue, L., Wang, X., Xu, C., Chen, T., Yang, L., Wang, T., Zhang, Q., and Wang, W.:  
997 Summertime fine particulate nitrate pollution in the North China Plain: increasing trends,  
998 formation mechanisms and implications for control policy, Atmos. Chem. Phys., 18, 11261-  
999 11275, 10.5194/acp-18-11261-2018, 2018.

1000 Wolfe, G. M., Marvin, M. R., Roberts, S. J., Travis, K. R., and Liao, J.: The Framework for 0-  
1001 D Atmospheric Modeling (F0AM) v3.1, Geosci. Model Dev., 9, 3309-3319, 10.5194/gmd-9-  
1002 3309-2016, 2016.

1003 Womack, C. C., McDuffie, E. E., Edwards, P. M., Bares, R., de Gouw, J. A., Docherty, K. S.,  
1004 Dube, W. P., Fibiger, D. L., Franchin, A., Gilman, J. B., Goldberger, L., Lee, B. H., Lin, J. C.,  
1005 Long, R., Middlebrook, A. M., Millet, D. B., Moravek, A., Murphy, J. G., Quinn, P. K.,  
1006 Riedel, T. P., Roberts, J. M., Thornton, J. A., Valin, L. C., Veres, P. R., Whitehill, A. R., Wild,  
1007 R. J., Warneke, C., Yuan, B., Baasandorj, M., and Brown, S. S.: An odd oxygen framework  
1008 for wintertime ammonium nitrate aerosol pollution in urban areas: NO<sub>x</sub> and VOC control as  
1009 mitigation strategies, Geophysical Research Letters, 0, 10.1029/2019gl082028, 2019.

1010 Wu, C., Wang, C., Wang, S., Wang, W., Yuan, B., Qi, J., Wang, B., Wang, H., Wang, C., Song,

1011 W., Wang, X., Hu, W., Lou, S., Ye, C., Peng, Y., Wang, Z., Huangfu, Y., Xie, Y., Zhu, M.,  
1012 Zheng, J., Wang, X., Jiang, B., Zhang, Z., and Shao, M.: Measurement report: Important  
1013 contributions of oxygenated compounds to emissions and chemistry of volatile organic  
1014 compounds in urban air, *Atmos. Chem. Phys.*, 20, 14769-14785, 10.5194/acp-20-14769-2020,  
1015 2020.

1016 Xu, L., and Penner, J. E.: Global simulations of nitrate and ammonium aerosols and their  
1017 radiative effects, *Atmos. Chem. Phys.*, 12, 9479-9504, 10.5194/acp-12-9479-2012, 2012.

1018 Xue, J., Yuan, Z., Lau, A. K. H., and Yu, J. Z.: Insights into factors affecting nitrate in PM<sub>2.5</sub>  
1019 in a polluted high NO<sub>x</sub> environment through hourly observations and size distribution  
1020 measurements, *Journal of Geophysical Research: Atmospheres*, 119, 4888-4902,  
1021 10.1002/2013JD021108, 2014a.

1022 Xue, L. K., Wang, T., Gao, J., Ding, A. J., Zhou, X. H., Blake, D. R., Wang, X. F., Saunders,  
1023 S. M., Fan, S. J., Zuo, H. C., Zhang, Q. Z., and Wang, W. X.: Ground-level ozone in four  
1024 Chinese cities: precursors, regional transport and heterogeneous processes, *Atmos. Chem.*  
1025 *Phys.*, 14, 13175-13188, 10.5194/acp-14-13175-2014, 2014b.

1026 Yang, Q., Su, H., Li, X., Cheng, Y., Lu, K., Cheng, P., Gu, J., Guo, S., Hu, M., and Zeng, L.:  
1027 Daytime HONO formation in the suburban area of the megacity Beijing, China, *Science*  
1028 *China Chemistry*, 57, 1032-1042, 2014.

1029 Yang, T., Sun, Y., Zhang, W., Wang, Z., Liu, X., Fu, P., and Wang, X.: Evolutionary processes  
1030 and sources of high-nitrate haze episodes over Beijing, Spring, *Journal of Environmental*  
1031 *Sciences*, 54, 142-151, <https://doi.org/10.1016/j.jes.2016.04.024>, 2017.

1032 Ye, C., Gao, H., Zhang, N., and Zhou, X.: Photolysis of Nitric Acid and Nitrate on Natural  
1033 and Artificial Surfaces, *Environmental Science & Technology*, 50, 3530-3536,  
1034 10.1021/acs.est.5b05032, 2016.

1035 Ye, C., Zhang, N., Gao, H., and Zhou, X.: Photolysis of Particulate Nitrate as a Source of  
1036 HONO and NO<sub>x</sub>, *Environmental Science & Technology*, 51, 6849-6856,  
1037 10.1021/acs.est.7b00387, 2017.

1038 Ye, C., Yuan, B., Lin, Y., Wang, Z., Hu, W., Li, T., Chen, W., Wu, C., Wang, C., Huang, S., Qi,  
1039 J., Wang, B., Wang, C., Song, W., Wang, X., Zheng, E., Krechmer, J. E., Ye, P., Zhang, Z.,  
1040 Wang, X., Worsnop, D. R., and Shao, M.: Chemical characterization of oxygenated organic  
1041 compounds in the gas phase and particle phase using iodide CIMS with FIGAERO in urban  
1042 air, *Atmospheric Chemistry and Physics*, 21, 8455-8478, 10.5194/acp-21-8455-2021, 2021.

1043 Yu, C., Wang, Z., Xia, M., Fu, X., Wang, W., Tham, Y. J., Chen, T., Zheng, P., Li, H., Shan, Y.,  
1044 Wang, X., Xue, L., Zhou, Y., Yue, D., Ou, Y., Gao, J., Lu, K., Brown, S. S., Zhang, Y., and  
1045 Wang, T.: Heterogeneous N<sub>2</sub>O<sub>5</sub> reactions on atmospheric aerosols at four Chinese sites:  
1046 improving model representation of uptake parameters, *Atmos. Chem. Phys.*, 20, 4367-4378,  
1047 10.5194/acp-20-4367-2020, 2020.

1048 Yu, Y., Cheng, P., Li, H., Yang, W., Han, B., Song, W., Hu, W., Wang, X., Yuan, B., Shao, M.,  
1049 Huang, Z., Li, Z., Zheng, J., Wang, H., and Yu, X.: Budget of nitrous acid (HONO) and its  
1050 impacts on atmospheric oxidation capacity at an urban site in the fall season of Guangzhou,  
1051 China, *Atmos. Chem. Phys. Discuss.*, 2021, 1-38, 10.5194/acp-2021-178, 2021.

1052 Yuan, B., Chen, W., Shao, M., Wang, M., Lu, S., Wang, B., Liu, Y., Chang, C., and Wang, B.:  
1053 Measurements of ambient hydrocarbons and carbonyls in the Pearl River Delta (PRD), China,  
1054 *Atmospheric Research*, 116, 93-104, 2012.

1055 Yuan, B., Liggio, J., Wentzell, J., Li, S. M., Stark, H., Roberts, J. M., Gilman, J., Lerner, B.,  
1056 Warneke, C., Li, R., Leithead, A., Osthoff, H. D., Wild, R., Brown, S. S., and de Gouw, J. A.:  
1057 Secondary formation of nitrated phenols: insights from observations during the Uintah Basin  
1058 Winter Ozone Study (UBWOS) 2014, *Atmos. Chem. Phys.*, 16, 2139-2153, 10.5194/acp-16-  
1059 2139-2016, 2016.

1060 Yun, H., Wang, T., Wang, W., Tham, Y. J., Li, Q., Wang, Z., and Poon, S. C. N.: Nighttime  
1061 NO<sub>x</sub> loss and ClNO<sub>2</sub> formation in the residual layer of a polluted region: Insights from field  
1062 measurements and an iterative box model, *Science of The Total Environment*, 622-623, 727-  
1063 734, <https://doi.org/10.1016/j.scitotenv.2017.11.352>, 2018a.

1064 Yun, H., Wang, W., Wang, T., Xia, M., Yu, C., Wang, Z., Poon, S. C. N., Yue, D., and Zhou,  
1065 Y.: Nitrate formation from heterogeneous uptake of dinitrogen pentoxide during a severe  
1066 winter haze in southern China, *Atmos. Chem. Phys.*, 18, 17515-17527, 10.5194/acp-18-  
1067 17515-2018, 2018b.

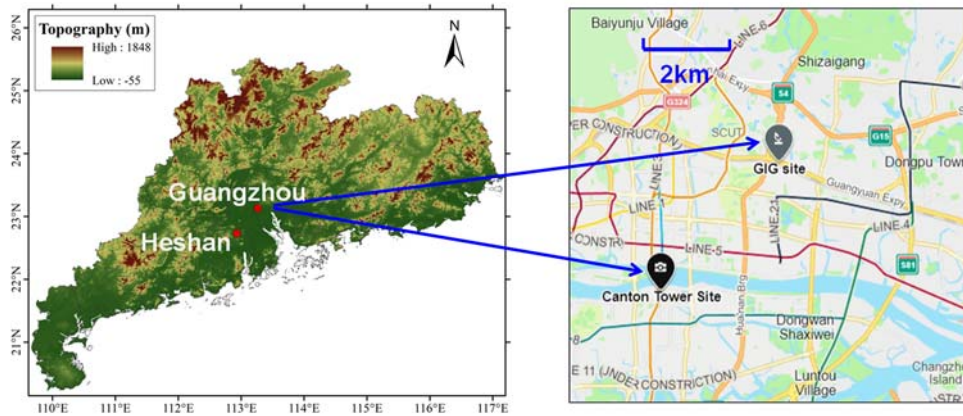
1068 Zhai, S., Jacob, D. J., Wang, X., Liu, Z., Wen, T., Shah, V., Li, K., Moch, J. M., Bates, K. H.,  
1069 Song, S., Shen, L., Zhang, Y., Luo, G., Yu, F., Sun, Y., Wang, L., Qi, M., Tao, J., Gui, K., Xu,  
1070 H., Zhang, Q., Zhao, T., Wang, Y., Lee, H. C., Choi, H., and Liao, H.: Control of particulate  
1071 nitrate air pollution in China, *Nature Geoscience*, 10.1038/s41561-021-00726-z, 2021.

1072 Zhang, H., An, Q., Zhao, S., Xie, B., and Liu, Q.: Advances in the research of optical  
1073 properties and radiative forcing of nitrate aerosols, *Acta Meteorologica Sinica*, 75, 539-551,  
1074 2017.

1075 Zhang, R., Gen, M., Huang, D., Li, Y., and Chan, C. K.: Enhanced Sulfate Production by  
1076 Nitrate Photolysis in the Presence of Halide Ions in Atmospheric Particles, *Environmental  
1077 Science & Technology*, 54, 3831-3839, 10.1021/acs.est.9b06445, 2020.

1078 Zhou, S., Wu, L., Guo, J., Chen, W., Wang, X., Zhao, J., Cheng, Y., Huang, Z., Zhang, J., Sun,  
1079 Y., Fu, P., Jia, S., Tao, J., Chen, Y., and Kuang, J.: Measurement report: Vertical distribution  
1080 of atmospheric particulate matter within the urban boundary layer in southern China – size-  
1081 segregated chemical composition and secondary formation through cloud processing and  
1082 heterogeneous reactions, *Atmos. Chem. Phys.*, 20, 6435-6453, 10.5194/acp-20-6435-2020,  
1083 2020.

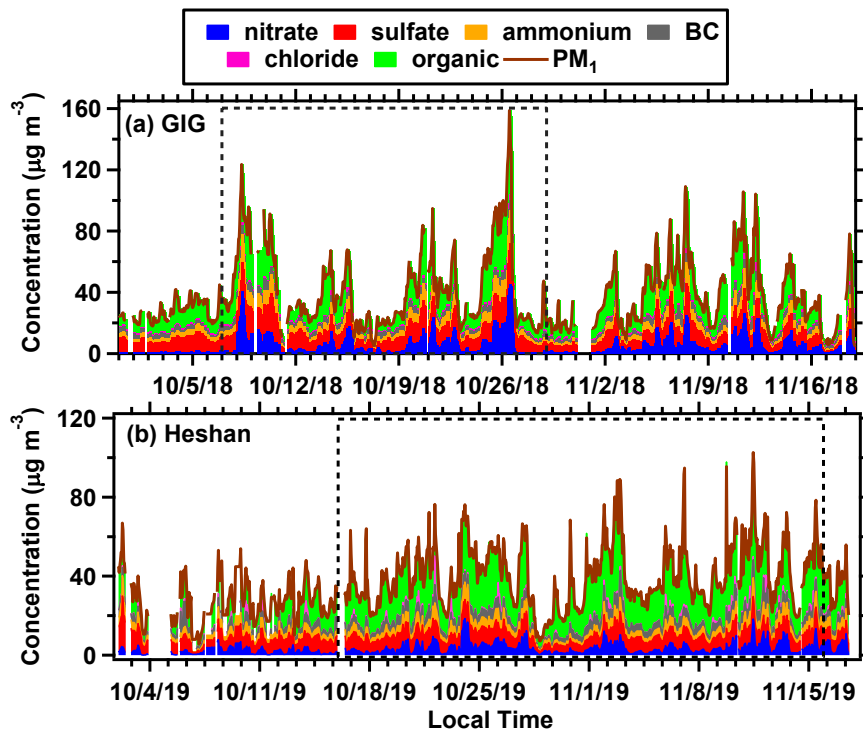




1084

1085 **Figure 1.** Sampling site at Guangzhou Institute of Geochemistry, Chinese Academy of  
 1086 Sciences (GIG), Heshan and Canton Tower. Note that the map is extracted from  
 1087 Microsoft Bing maps by the authors.

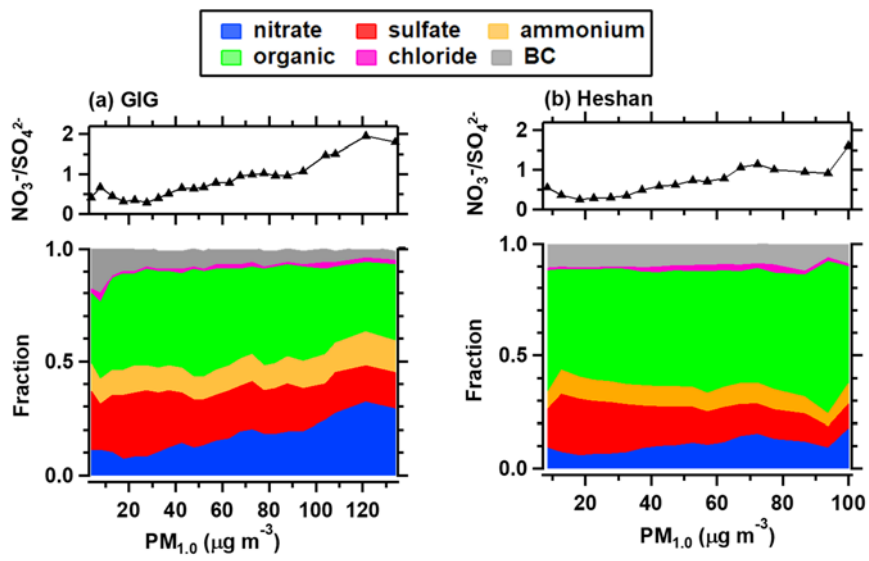
1088



1090

1091 **Figure 2.** Temporal variations of the mass concentration of the major chemical  
 1092 components in PM<sub>1</sub> including nitrate (NO<sub>3</sub><sup>-</sup>), sulfate (SO<sub>4</sub><sup>2-</sup>), ammonium (NH<sub>4</sub><sup>+</sup>), black  
 1093 carbon (BC), chloride (Cl<sup>-</sup>) and organics at (a) GIG site and (b) Heshan site. The black  
 1094 dashed rectangle represents the investigated period which had complete set of data.

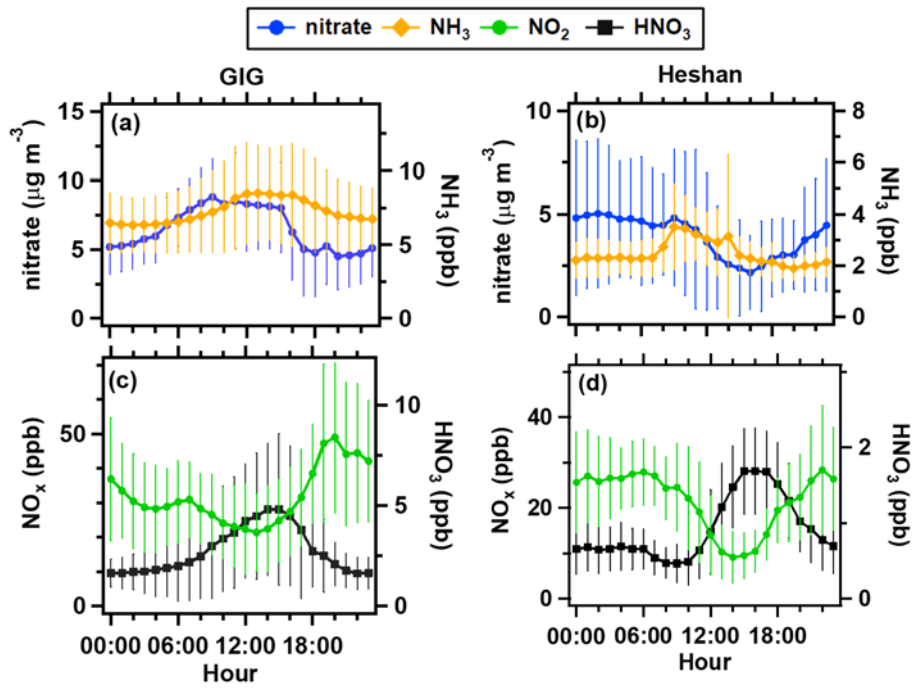
1095



1097

1098 **Figure 3.** The mass concentration ratio of  $\text{NO}_3^-/\text{SO}_4^{2-}$  (top) and fractions of major  
 1099 chemical components (bottom) in  $\text{PM}_1$  at (a) GIG site and (b) Heshan site.

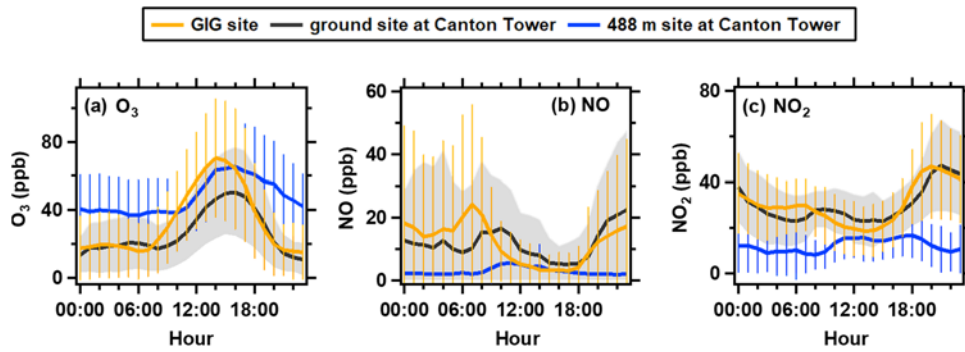
1100



1101

1102 **Figure 4.** Diurnal variations of mean concentrations of nitrate and related pollution  
 1103 species at (a) GIG site and (b) Heshan site. The error bars represent the standard  
 1104 deviation of the means.

1105

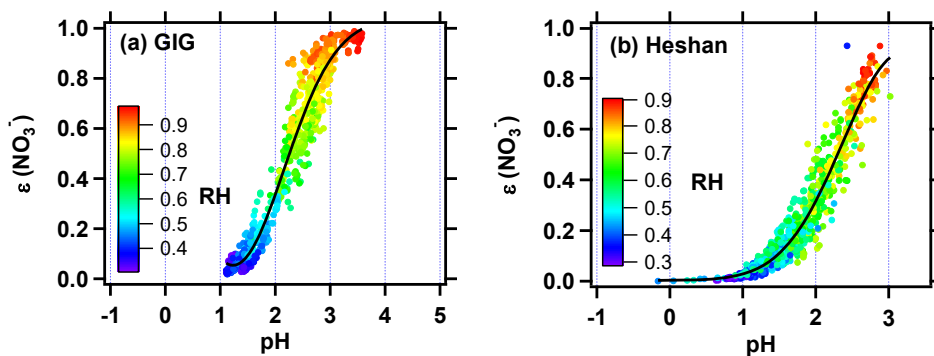


1107

1108 **Figure 5.** Diurnal variation of mean concentrations of (a) O<sub>3</sub>, (b) NO, (c) NO<sub>2</sub> at GIG  
 1109 (orange lines), and the ground and 488m sites of Canton Tower (black and blue lines,  
 1110 respectively). The orange and blue error bars represent the standard deviations of the  
 1111 mean concentrations at the GIG site and the 488m site of Canton Tower, the grey areas  
 1112 show one standard deviation of the mean concentration at ground site of Canton Tower.

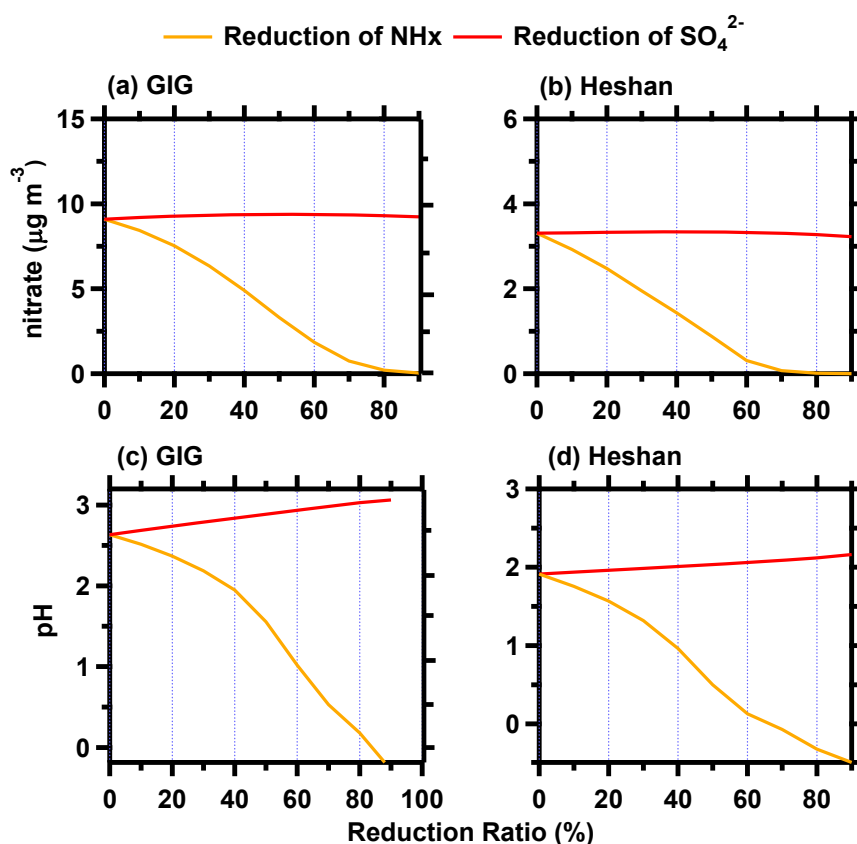
1113

1114



1115

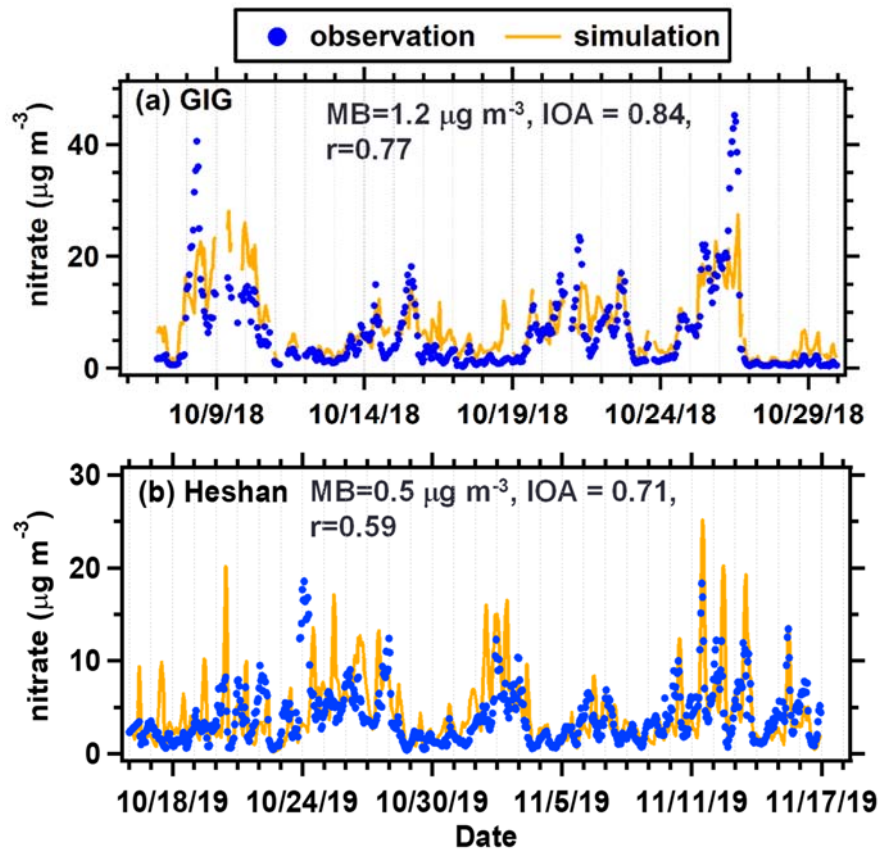
1116 **Figure 6.** The particle fraction of nitrate in the sum of HNO<sub>3</sub>+nitrate ( $\epsilon(\text{NO}_3^-)$ ) against  
 1117 aerosol pH. The pH data are colored by relative humidity and fit to an “s-curve” in  
 1118 black line, as shown in Guo et al. (2018).



1119

1120 **Figure 7.** ISORROPIA-predicted average nitrate (a, b) and pH (c, d) as a function of  
 1121 changes in NH<sub>x</sub> (ammonium + NH<sub>3</sub>, orange line) and SO<sub>4</sub><sup>2-</sup> (red line) at the GIG and  
 1122 Heshan site during the study period.

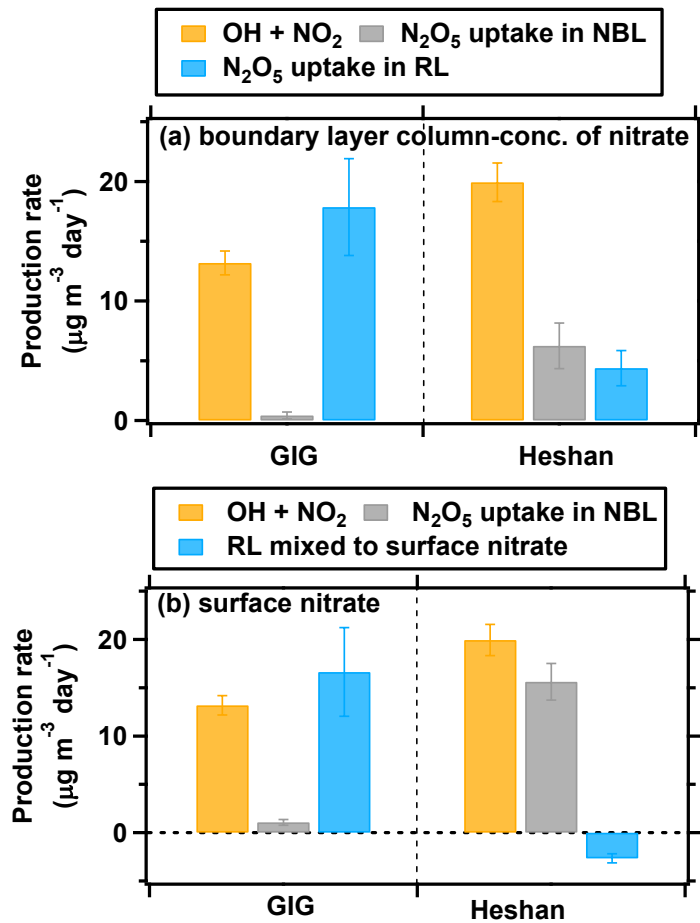
1123



1125

1126 **Figure 8.** Comparison of the temporal box model simulated and observed nitrate at the  
1127 (a) GIG site and (b) Heshan site.

1128

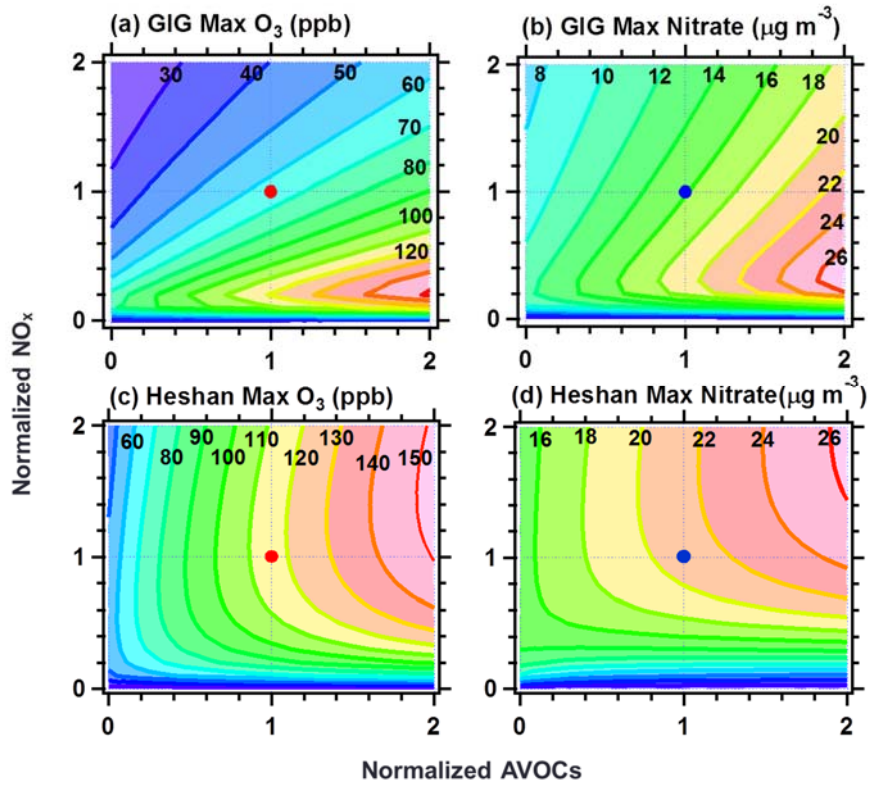


1129

1130 **Figure 9.** The daily-averaged contribution (a) to boundary layer column concentration  
 1131 and (b) to surface nitrate from three pathways (OH +NO<sub>2</sub> reaction, N<sub>2</sub>O<sub>5</sub> uptake in NBL,  
 1132 and N<sub>2</sub>O<sub>5</sub> uptake in RL/N<sub>2</sub>O<sub>5</sub> uptake from RL mixed process) at the GIG and Heshan  
 1133 sites. The error bars represent the standard deviations of the mean production rate.

1134

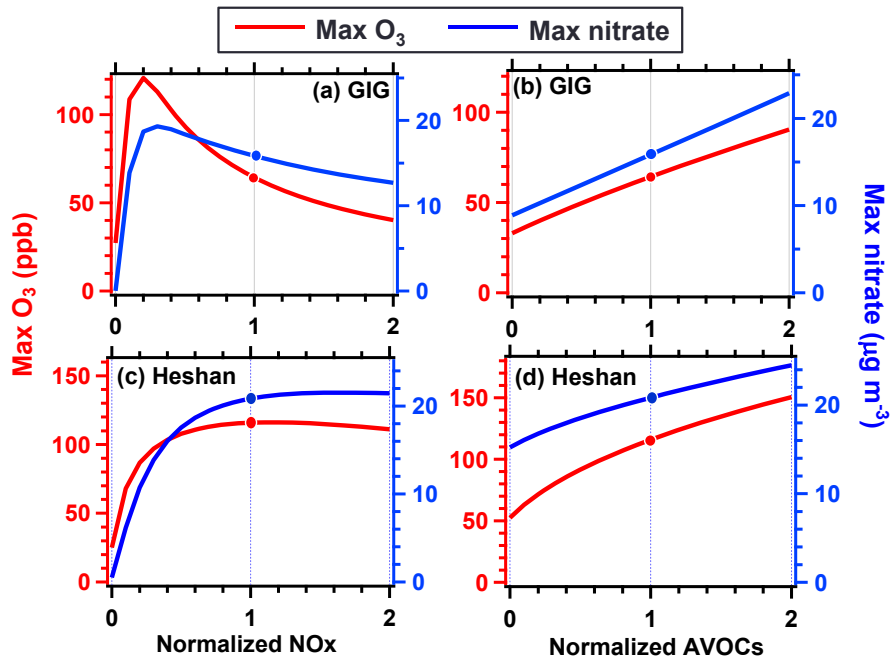




1136

1137 **Figure 10.** The simulated isopleths of ozone and nitrate with normalized NO<sub>x</sub> and  
 1138 AVOCs concentration at the (a, b) GIG site and (c, d) Heshan site, each isopleth  
 1139 represents the maximum ozone and nitrate in the simulation, and the red and blue circles  
 1140 represent the base cases.

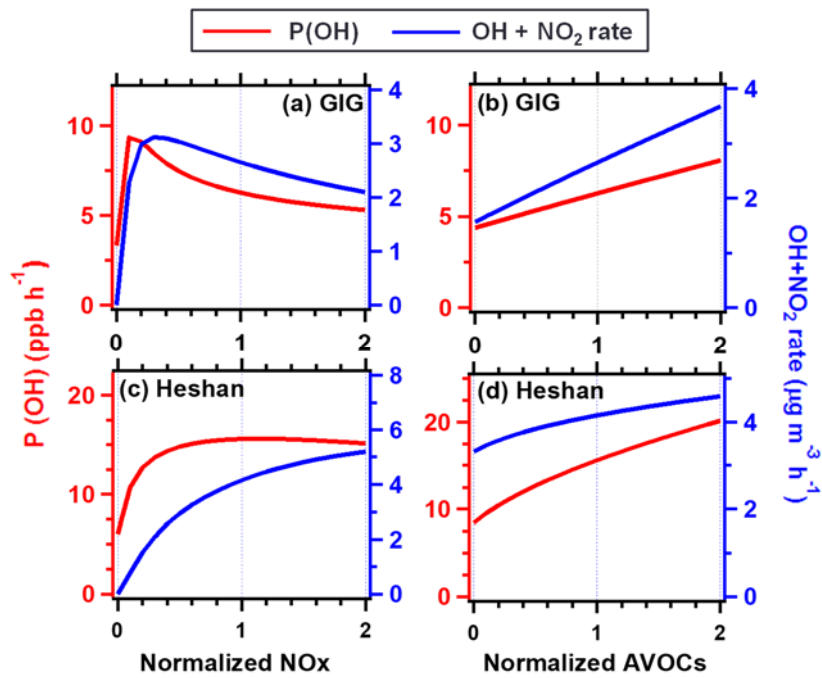
1141



1142

1143 **Figure 11.** Simulated maximum ozone and nitrate concentration with normalized  
 1144 NO<sub>x</sub> and AVOCs at the (a, b) GIG site and (c, d) Heshan site, cutting through the  
 1145 simulated isopleth in Figure 8 with normalized AVOCs and NO<sub>x</sub> ratio at 1, respectively.  
 1146 The red and blue circles represent the base cases.

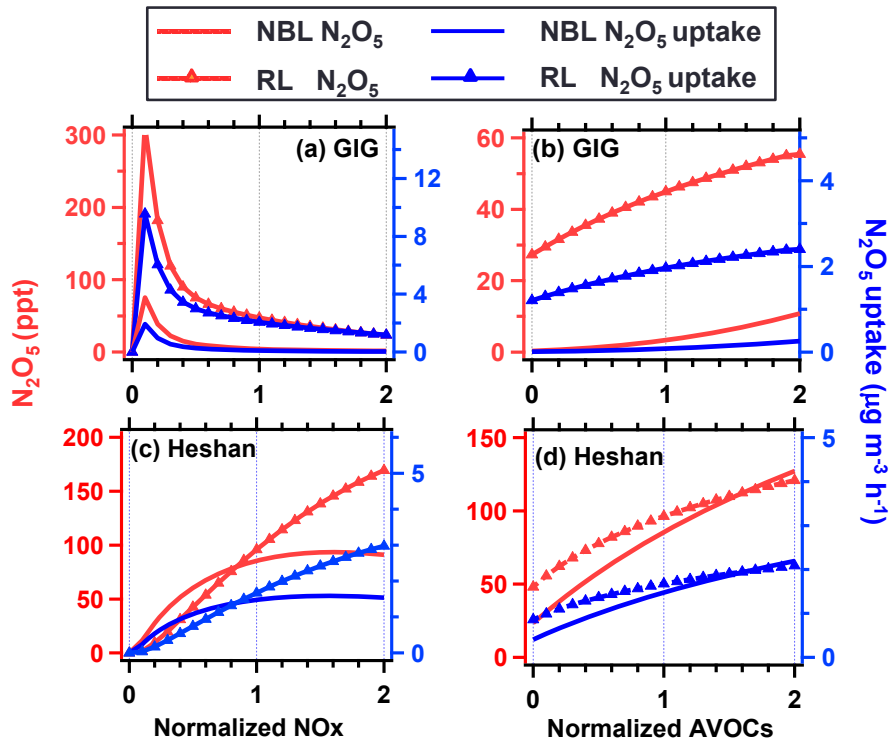
1147



1148

1149 **Figure 12.** Simulated average production rates of OH ( $P(OH)$ ) and the reaction rate of  
 1150 OH and  $NO_2$  with the normalized changes of  $NO_x$  and AVOCs emissions at the (a, b)  
 1151 GIG site and (c, d) Heshan site.

1152



1153

1154 **Figure 13.** Simulated average concentration of  $N_2O_5$  and nitrate production rate from  
 1155  $N_2O_5$  uptake with the normalized changes of  $NO_x$  and AVOCs emissions at the (a, b)  
 1156 GIG site and (c, d) Heshan site in the NBL and RL.

1157